J. Fluid Mech. (1997), *vol.* 346, *pp.* 239–270. Printed in the United Kingdom

A frictional–kinetic model for the flow of granular materials through a wedge-shaped hopper

By R. JYOTSNA AND K. KESAVA RAO

Department of Chemical Engineering, Indian Institute of Science, Bangalore 560012, India
e-mail: kesava@chemeng.iisc.ernet.in

(Received 10 March 1994 and in revised form 18 April 1997)

A quasi-one-dimensional model is used to examine the steady flow of granular materials through a wedge-shaped hopper with smooth, steep walls. Hybrid frictional–kinetic equations are used in an attempt to overcome some of the difficulties faced by earlier works, which were based on frictional equations. Owing to computational difficulties, two different solution procedures are used: (i) in the upper region, where frictional effects dominate, and (ii) the lower region which includes the exit slot and a part of the particle jet below the hopper, where kinetic and frictional effects are expected to be comparable. The equations are integrated numerically in (i). In (ii), they are linearized, and a semi-analytical solution is constructed. In contrast to the works of Kaza & Jackson (1982*a*) and Prakash & Rao (1991), the density varies smoothly across the exit slot. The density profile is qualitatively similar to the data of Fickie, Mehrabi & Jackson (1989). However, the range of density variation is much smaller than that observed. Owing to the approximations used, and perhaps also to the form of the kinetic constitutive equations, kinetic effects are dominated by frictional effects, except close to the downstream boundary.

1. Introduction

Theoretical studies of granular flow have often been based on frictional constitutive equations. These equations were first developed to model the slow flow of granular materials at high bulk densities, where the stresses developed are mainly due to contact between the constituent grains which rub against each other as they flow (Jenike 1961; Brown & Richards 1970; Spencer 1982; Nedderman *et al.* 1982; Jackson 1983). They are based on the principles of metal plasticity and soil mechanics. In practical flow situations, bulk densities in certain regions may decrease to levels where the particles are no longer in sustained contact with each other. At such densities, as frictional stresses are not expected to play a major role, it is incorrect to use frictional theories alone to model the flow.

In the past few years, considerable effort has been directed towards the development of constitutive theories for granular flow at high shear rates and low bulk densities (McTigue 1978; Savage & Jeffrey 1981; Ackermann & Shen 1982; Jenkins & Savage 1983; Ahmadi & Shahinpoor 1984; Lun *et al.* 1984; Jenkins & Richman 1985; Lun & Savage 1987; Ma & Ahmadi 1988; Boyle & Massoudi 1990; Lun 1991; Potanin 1992; Goldshtein & Shapiro 1995). They are based on the idea that stresses in this regime are due to the momentum transfer associated with interparticle collisions, and with the transport of particles between collisions. Since they have been developed by

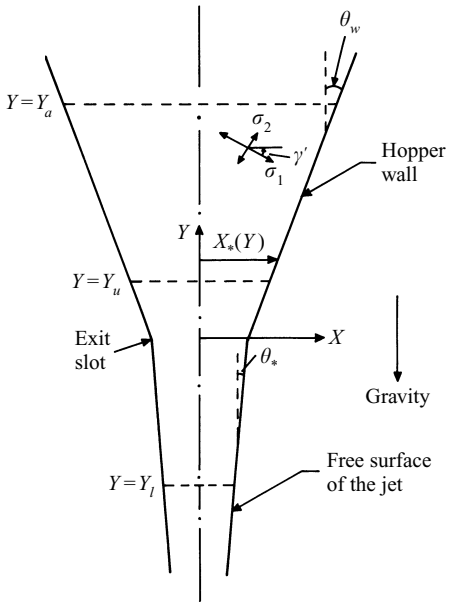

FIGURE 1. Cartesian coordinate system for hopper flow. Here $X = x/w$ and $Y = y/w$ are the dimensionless x- and y-coordinates, w is the half-width of the exit slot, and σ_1 and σ_2 are the major and minor principal frictional stresses, respectively, in the (x, y)-plane.

analogy with the kinetic theory of dense gases, we refer to them as kinetic theories for granular materials.

These theories have been used to study simple shear flow between parallel plates (Haff 1983; Lun *et al.* 1984; Ma & Ahmadi 1988), inclined chute flow (Szidarovszky, Hutter & Yakowitz 1987; Anderson & Jackson 1992; Cao, Ahmadi & Massoudi 1996), flow in gas fluidized beds (Ding & Gidaspow 1990) and flow in vibrated beds (Potanin 1992; Goldshtein *et al.* 1995). They have also been combined with the frictional theories to examine flow through inclined chutes (Savage 1983; Johnson, Nott & Jackson 1990; Anderson & Jackson 1992), plane shear between parallel plates (Johnson & Jackson 1987), and particle motions in vibrated beds (Savage 1988). Some phenomenological theories have also been used to model flows through inclined chutes and vertical channels (Goodman & Cowin 1971; Passman, Jenkins & Thomas 1978; Savage 1979; Sayed & Savage 1983; Yalamanchili, Gudhe & Rajagopal 1994).

However, except for the preliminary analysis of Kaza (1982), and our analysis of a simple one-dimensional approximation (Jyotsna & Rao 1991), the attempts have not been extended to hopper flow.

A hopper is a vessel which is commonly used in the storage and handling of granular materials. Here we consider a wedge-shaped hopper, which is of rectangular cross-section, and whose elevation is shown in figure 1. For steady flow of material through the hopper, it is desired to predict the stress, density, and velocity fields. Though this problem has been examined for three decades (Savage 1965; Davidson & Nedderman 1973; Brennen & Pearce 1978; Kaza & Jackson 1982*a*, *b*; Meric & Tabarrok 1982; Prakash & Rao 1991), there is no solution whose predictions agree closely with the observed mass flow rates and density profiles.

The analyses cited above are based on frictional constitutive equations. In the

vicinity of the exit slot, henceforth referred to as the exit region, the solutions lead to various mathematical and physical difficulties (Kaza & Jackson 1982*a*, *b*; 1984; Prakash & Rao 1991). Some of these are indicated in § 6.1.

Hence it appears that the constitutive equations should be modified. As noted by Jyotsna & Rao (1991), density measurements (Bosley, Schofield & Shook 1969; Van Zuilichem, Van Egmond & De Swart 1974; Fickie, Mehrabi & Jackson 1989) show that the material dilates as it flows down the hopper. In the exit region, the density may be low enough for kinetic effects to be important relative to frictional effects. Indeed, Darton (1976) suggested that collisional or kinetic effects may be important in the particle jet below the hopper. On the other hand, frictional effects are likely to dominate in the upper region of the hopper, where the density is high. Therefore, a frictional-kinetic model may overcome some of the defects associated with the frictional model.

Here we use a hybrid frictional–kinetic model to examine steady compressible flow through a wedge-shaped hopper. To simplify the analysis, it is assumed that the walls are smooth and the flow is two-dimensional. The latter assumption implies that the dependent variables do not vary in the z-direction, which is perpendicular to the plane of the paper in figure 1.

The present work is an extension of our earlier study (Jyotsna & Rao 1991), where the solution of a one-dimensional approximation called the smooth-wall, radial gravity (SWRG) problem was obtained. An approximate solution was constructed for the special case of incompressible flow, with gravity taken to be directed radially towards the apparent vertex of the hopper. Here we retain the assumption of smooth walls, but attempt to solve the more realistic two-dimensional problem, with vertical gravity and density variation. It is hoped that the use of a frictional–kinetic model may eliminate at least some of the problems encountered by frictional models in the exit region.

The structure of the governing partial differential equations requires the specification of boundary conditions at the downstream boundary. As satisfactory conditions at the hopper exit have not yet been proposed, the particle jet is included in the analysis, and plausible downstream conditions are specified some distance below the exit. Barring the work of Hankey & Thomas (1991) (discussed later), there do not appear to have been any attempts to solve simultaneously for the flow field in the hopper and in the particle jet below.

One source of difficulty must be noted. Some distance below the exit, air drag becomes important. It is possible to include air drag, or more generally, fluid–particle interactions in the present analysis. However, as the flows of fluid and particles are coupled, the number of equations to be solved simultaneously increases considerably. The effects of air drag have been neglected here in order to simplify the analysis. Thus the present work may be regarded as a precursor to the eventual introduction of fluid–particle interactions into the frictional–kinetic model.

Our preliminary attempts to solve the equations for steady two-dimensional flow were unsuccessful. Therefore it was decided to examine a simpler quasi-one-dimensional model, obtained by suitably averaging the two-dimensional equations. In order to understand the simplification, we first present the two-dimensional equations.

2. Problem formulation for steady two-dimensional flow

2.1. *Governing equations in Cartesian coordinates*

It is convenient to express the equations in terms of the dimensionless variables

$$\left.\begin{aligned} X = \frac{x}{w}; \quad Y = \frac{y}{w}; \quad v = \frac{\rho}{\rho_p}; \quad U = \frac{v_x}{(gw)^{1/2}}; \quad V = \frac{v_y}{(gw)^{1/2}}; \\ \sigma' = \frac{\sigma}{\rho_p g w}; \quad \tau' = \frac{\tau}{\rho_p g w}; \quad T' = \frac{T}{g d_p^2/w}, \end{aligned}\right\} \tag{1}$$

where w is the half-width of the exit slot (figure 1), ρ_p is the density of the solid, g is the acceleration due to gravity, v is the volume fraction of solids, v_x and v_y are the x- and y-components of velocity, and σ and τ are the mean and deviatoric frictional stresses, respectively, defined by

$$\sigma \equiv \frac{\sigma_1 + \sigma_2}{2} \;\; ; \;\; \tau \equiv \frac{\sigma_1 - \sigma_2}{2} \;\; ; \;\; \sigma_1 \geqslant \sigma_2. \tag{2}$$

Here σ_1 and σ_2 are the major and minor principal frictional stresses, respectively in the plane of flow, and T is the 'grain temperature' defined by

$$\tfrac{3}{2} T \;\equiv\; \tfrac{1}{2}\langle C^2 \rangle, \tag{3}$$

where $\boldsymbol{C} \equiv \boldsymbol{c} - \boldsymbol{v}$ is the peculiar velocity of a particle with velocity $\boldsymbol{c}$, and $\boldsymbol{v}$ is the mean velocity of the collection of particles. The angular brackets in (3) denote an ensemble average based on the single-particle velocity distribution function. Thus T is proportional to the 'pseudo-thermal' energy, or mean kinetic energy per unit mass of velocity fluctuations.

Details of the frictional and kinetic constitutive theories used are given in Prakash & Rao (1988) and Jyotsna & Rao (1991), respectively, and are therefore not discussed in detail here.

It suffices to note that the components of the frictional consitutive equations are the yield condition, the coaxiality condition, and the flow rule (see also Jackson 1983 and Pitman & Schaeffer 1987). The yield condition provides a relation between the solids fraction v and the components of the stress tensor. The coaxiality condition implies that the principal axes of the stress and the rate of deformation tensors are aligned, and the flow rule relates the rate of dilation to the stresses.

The kinetic constitutive equations provide expressions for the stresses arising from particle collisions and transport, the flux of the kinetic energy associated with velocity fluctuations, and the rate of dissipation of this energy into heat due to inelastic interparticle collisions. The constitutive equations are taken from Lun *et al.* (1984).

Finally, we assume that the stress tensor $\boldsymbol{\sigma}$ is given by $\boldsymbol{\sigma} = \boldsymbol{\sigma}^f + \boldsymbol{\sigma}^k$, where the superscripts f and k refer to the frictional and kinetic contributions, respectively. The assumption that the stress tensor can be represented as the sum of a rate-independent or 'frictional' part and a rate-dependent or 'viscous' part is due to Goodman & Cowin (1971). Subsequently, Savage (1983) suggested the use of equations based on kinetic theory for the rate-dependent part.

The dimensionless balance laws are given by:

mass balance

$$\frac{\partial}{\partial X}(vU) + \frac{\partial}{\partial Y}(vV) = 0, \tag{4}$$

momentum balance (X-component)

$$\frac{\partial(\nu U U)}{\partial X}+\frac{\partial(\nu V U)}{\partial Y}+\frac{\partial \sigma_{XX}}{\partial X}+\frac{\partial \sigma_{XY}}{\partial Y}=0, \tag{5}$$

momentum balance (Y-component)

$$\frac{\partial(\nu U V)}{\partial X}+\frac{\partial(\nu V V)}{\partial Y}+\frac{\partial \sigma_{XY}}{\partial X}+\frac{\partial \sigma_{YY}}{\partial Y}+\nu=0, \tag{6}$$

pseudo-thermal energy balance

$$\begin{aligned}\frac{3}{2}\left(\frac{\partial(\nu U T')}{\partial X}+\frac{\partial(\nu V T')}{\partial Y}\right)+\left(\frac{\partial q_X}{\partial X}+\frac{\partial q_Y}{\partial Y}\right)\\ +\left(\frac{\partial U}{\partial X}+\frac{\partial V}{\partial Y}\right)\left[T' h_1-T'^{1/2}\,\bar{h}_2\left(\frac{\partial U}{\partial X}+\frac{\partial V}{\partial Y}\right)\right]-2T'^{1/2}h_3\\ \times\left[\left(\frac{\partial U}{\partial X}\right)^2+\left(\frac{\partial V}{\partial Y}\right)^2+\frac{1}{2}\left(\frac{\partial U}{\partial Y}+\frac{\partial V}{\partial X}\right)^2\right]+D=0,\end{aligned} \tag{7}$$

where the stresses in (5) and (6) are given by

$$\left.\begin{aligned}\sigma_{XX}&=\sigma'+\tau'\cos 2\gamma'+\epsilon T'^{1/2}\left[T'^{1/2}h_1-\bar{h}_2\left(\frac{\partial U}{\partial X}+\frac{\partial V}{\partial Y}\right)-2h_3\frac{\partial U}{\partial X}\right],\\ \sigma_{XY}&=-\tau'\sin 2\gamma'-\epsilon T'^{1/2}h_3\left(\frac{\partial U}{\partial Y}+\frac{\partial V}{\partial X}\right),\\ \sigma_{YY}&=\sigma'-\tau'\cos 2\gamma'+\epsilon T'^{1/2}\left[T'^{1/2}h_1-\bar{h}_2\left(\frac{\partial U}{\partial X}+\frac{\partial V}{\partial Y}\right)-2h_3\frac{\partial V}{\partial Y}\right].\end{aligned}\right\} \tag{8}$$

The frictional contributions in (8) are identified by the appearance of σ' and τ', while the kinetic contributions involve T' and the functions $h_i(\nu,\eta)$. These functions are defined in table 1, and γ' is the angle between the σ_1-axis and the X-direction (figure 1). The functions $h_i(\nu,\eta)$ depend on $g_0(\nu)$, the radial distribution function at contact. Here g_0 is chosen as (Ma & Ahmadi 1986)

$$g_0=\frac{1+2.5\nu+4.5904\nu^2+4.515439\nu^3}{\left[1-\left(\nu/\nu_m\right)^3\right]^{0.67802}}, \tag{9}$$

where $\nu_m=0.64356$ is the solids fraction corresponding to random close packing. Equation (9) fits the simulation data of Alder & Wainwright (1960) very well at both low and high densities. As in the kinetic theory of gases, $\epsilon T' h_1$ is the pressure, and $\epsilon T'^{1/2}h_3$ and $\epsilon T'^{1/2}h_2$ are the shear and bulk viscosities, respectively.

In (7), q_X is the x-component of the flux of pseudo-thermal energy, and D is the rate of dissipation of pseudo-thermal energy per unit volume due to inelastic collistions. The expressions for q_X, q_Y, and D are

$$q_X=-\epsilon T'^{1/2}h_4\frac{\partial T'}{\partial X};\quad q_Y=-\epsilon T'^{1/2}h_4\frac{\partial T'}{\partial Y};\quad D=T'^{3/2}h_6. \tag{10}$$

In the work of Lun *et al.* (1984), q_X and q_Y also depend on terms which are proportional to $\nabla\nu$. These terms are omitted here as they are believed to be of a lower order than the terms which have been retained.

For typical values of the particle diameter d_p and the width $2w$ of the exit slot, the parameter $\epsilon\equiv(d_p/w)^2$ is $\ll 1$.

$$h_1(v,\eta) = v(1+4\eta v g_0)$$

$$h_2(v,\eta) = \frac{8\eta v^2 g_0}{3\pi^{1/2}}$$

$$\bar{h}_2(v,\eta) = h_2 - (2/3)h_3$$

$$h_2'(v,\eta) = h_2 + (4/3)h_3$$

$$h_3(v,\eta) = \frac{5\pi^{1/2}}{96\eta(2-\eta)}\left(\frac{1}{g_0}+\frac{8\eta v}{5}\right)\left(1+\frac{8\eta(3\eta-2)vg_0}{5}\right)+\frac{8\eta v^2 g_0}{5\pi^{1/2}}$$

$$h_4(v,\eta) = \frac{25\pi^{1/2}}{16\eta(41-33\eta)}\left[\left(\frac{1}{g_0}+\frac{12\eta v}{5}\right)\left(1+\frac{12\eta^2(4\eta-3)vg_0}{5}\right)+\frac{64(41-33\eta)\eta^2 v^2 g_0}{25\pi}\right]$$

$$h_6(v,\eta) = \frac{48\eta(1-\eta)v^2 g_0}{\pi^{1/2}}$$

TABLE 1. The functions $h_i(v,\eta)$ in (7), (8), and (10): v = volume fraction of solids, $\eta \equiv \frac{1}{2}(1+e_p)$, e_p = coefficient of restitution for interparticle collisions, assumed constant, and $g_0(v)$ = equilibrium radial distribution function at contact.

The frictional stresses are given by

$$\sigma' = \alpha\sigma_c'(v); \quad \tau' = \sigma_c'(v)f(\alpha); \quad \alpha \equiv \frac{\sigma}{\sigma_c} = \frac{\sigma'}{\sigma_c'}, \tag{11}$$

where σ_c' is the dimensionless mean frictional stress at a critical state, given by

$$\sigma_c' = \beta \exp\left(\frac{\Gamma_1 - (1/v)}{\lambda_1}\right); \quad \beta \equiv \frac{p_a}{\rho_p g w}, \tag{12a,b}$$

and $f(\alpha)$ is obtained from the yield condition used by Prakash & Rao (1988)

$$f(\alpha) = \sin\phi\left(n\alpha - (n-1)\alpha^{n/(n-1)}\right). \tag{13}$$

Here $p_a = 101.33\,\mathrm{kN\ m^{-2}}$ is the atmospheric pressure, used as a non-dimensionalizing parameter, and Γ_1, λ_1, n, and the angle of internal friction ϕ are material constants.

From (12*a*), σ_c', the frictional mean stress at a critical state, is zero only at $v = 0$. However, Richardson (1971, pp. 51–52) reports that the solids fraction at minimum fluidization, where the particles lose contact with each other, is usually in the range 0.58–0.62. Further, Onoda & Liniger (1990) attempted to determine the volume fraction of solids corresponding to the loosest random packing that is stable. Their estimate, based on sedimentation and shearing experiments with closely graded glass spheres, is $v \simeq 0.56$. The recent computer simulations of Nolan & Kavanagh (1992) suggest a lower value of $v \simeq 0.509$. Below the density corresponding to loosest random packing, the use of a frictional contribution to the stress is incorrect. To correct the constitutive theory for this defect, the expression for $\sigma_c'(v)$ is modified. A cubic fit is used for $\sigma_c'(v)$ near $v = v_{min}$, where v_{min} is the solids fraction below which sustained contact between the grains is expected to be absent. In the present work, v_{min} is chosen as 0.5. This value has also been used by Johnson *et al.* (1990) in their work on chute

flow, and turns out to be close to the estimate of Nolan & Kavanagh (1992). Here the coefficients of the cubic are determined so that both σ_c' and $(\mathrm{d}\sigma_c'/\mathrm{d}v)$ vanish at $v = v_{min}$, and the values of σ_c' and $(\mathrm{d}\sigma_c'/\mathrm{d}v)$ at $v = v_1 > v_{min}$ match those obtained from (12). The value of v_1 is chosen by inspection, so that the function $\sigma_c'(v)$ shows a smooth transition to the cubic-fit region. Thus, the equation for σ_c' is modified to

$$\sigma_c' = \begin{cases} \beta \exp\left(\dfrac{\Gamma_1 - (1/v)}{\lambda_1}\right), & v \geqslant v_1 \\ (v - v_{min})^2\,(\sigma_{c1}(v - v_{min}) + \sigma_{c2}), & v_1 > v \geqslant v_{min} \\ 0, & v < v_{min}. \end{cases} \tag{14}$$

The form (12) is commonly used in soil mechanics (see for example Atkinson & Bransby 1978, pp. 239–240). As an alternative to (14), Rathbone, Nedderman & Davidson (1987) have used the first of (14) for $\sigma' > \sigma_*'$ and a linear relation between σ' and $1/v$ for $\sigma' < \sigma\,'_*$, where σ' is the frictional mean stress, and σ_*' is a constant. Jenike (1961, p. 12) assumed that $v = a(b + \sigma\,')^d$, where a, b, and d are constants.

Finally, (4)–(14) must be supplemented by the coaxiality condition and the flow rule. In Cartesian coordinates, these are given by:

coaxiality condition

$$\cos 2\gamma' \left(\frac{\partial U}{\partial Y} + \frac{\partial V}{\partial X}\right) - \sin 2\gamma' \left(\frac{\partial V}{\partial Y} - \frac{\partial U}{\partial X}\right) = 0, \tag{15}$$

flow rule

$$\cos 2\gamma' \left(\frac{\partial U}{\partial X} + \frac{\partial V}{\partial Y}\right) - \sin v_d \left(\frac{\partial V}{\partial Y} - \frac{\partial U}{\partial X}\right) = 0. \tag{16}$$

Here v_d is the angle of dilation, defined by

$$\sin v_d \equiv -(d_1 + d_2)\,/\,(d_1 - d_2)\,, \tag{17}$$

where d_1 and d_2 are the major and minor principal compressive rates of deformation, respectively. Since the divergence of the velocity field is given by $-(d_1 + d_2)$, it follows that the material dilates if $v_d > 0$, and vice versa. Further, for an 'associated' flow rule based on (11) and (13) (Prakash & Rao 1988), we have

$$\sin v_d \;=\; \frac{\partial \tau}{\partial \sigma} \;=\; n \sin\phi \left(1 - \alpha^{1/(n-1)}\right). \tag{18}$$

The variable v_d can be interpreted as an angle only if $|\sin v_d| \leqslant 1$.

Let us now determine the structure of the governing equations.

2.2. *Structure of the steady two-dimensional equations*

Using (11) and (13)–(18), the frictional variables σ', τ' and γ' may be expressed in terms of v and the velocity gradients. Equations (4)–(7) may then be written as a system of first-order equations of the form

$$\boldsymbol{E}\frac{\partial \boldsymbol{Z}}{\partial X} + \boldsymbol{F}\frac{\partial \boldsymbol{Z}}{\partial Y} = \boldsymbol{G}, \tag{19}$$

where

$$\boldsymbol{Z}^T = \left[v,\ \frac{\partial U}{\partial X},\ \frac{\partial U}{\partial Y},\ \frac{\partial V}{\partial X},\ \frac{\partial V}{\partial Y},\ \frac{\partial T'}{\partial X},\ \frac{\partial T'}{\partial Y}\right], \tag{20}$$

and the coefficient matrices $\boldsymbol{E}$ and $\boldsymbol{F}$ and the vector $\boldsymbol{G}$ depend on U, V, T', and $\boldsymbol{Z}$. The classification of (19) is based on the nature of the roots $(p_i, i = 1, 7)$ of the characteristic equation

$$\det\ (\boldsymbol{E}\ - p\ \boldsymbol{F})\ = (U - pV)\Delta_1(p^2 + 1) = 0, \tag{21}$$

where Δ_1 depends on U, V, T', and $\boldsymbol{Z}$.

If p_k is a real root of (21), there exists a characteristic curve in the (X, Y)-plane, defined by $\mathrm{d}Y/\mathrm{d}X = 1/p_k$. Equation (21) has one real root $p_1 = U/V$, and two imaginary roots $p_{6,7} = \pm i$, in addition to the roots p_2–p_5 of the equation $\Delta_1 = 0$.

The root p_1 arises from the mass balance (4), and the corresponding characteristic curve is a streamline. The roots p_6 and p_7 arise from the energy balance, and the roots $p_2 - p_5$ arise from the momentum balances. The nature of the latter roots depends on the value of ϵ.

Let us consider three cases.

(*a*) In the purely frictional case ((4)–(6) with $\epsilon = 0$ in (8)), (21) must be replaced by $(U - pV)\Delta_1 = 0$. Here p_2–p_5 correspond to two real double roots, provided provided $|\sin v_d| = |\partial\tau'/\partial\sigma'| \leqslant 1$ (Jackson 1983; Pitman & Schaeffer 1987).

(*b*) In the purely kinetic case, p_2–p_5 correspond to two imaginary double roots.

(*c*) The frictional–kinetic case with $\epsilon \ll 1$ is discussed below.

In case (*c*), the equation $\Delta_1 = 0$ is a quadratic in p^2. The leading term of the discriminant has the form $-\epsilon\,(H_1\,(1 - (\partial\tau'/\partial\sigma')^2) + H_2)$, where H_1 and H_2 are non-negative quantities. Hence a sufficient condition for the occurence of complex roots is $|\partial\tau'/\partial\sigma'| \leqslant 1$. This condition is satisfied along the dilation branch $(0 \leqslant \alpha = \sigma'/\sigma'_c \leqslant 1)$ of the yield condition (11), since (2) and (18) imply that $\partial\tau'/\partial\sigma' \leqslant n \sin\phi \leqslant 1$. It is also satisfied at points on the compaction branch $(\alpha > 1)$ which are sufficiently close to the critical state $(\alpha = 1)$. At other points where this condition is violated, the specific values of H_1 and H_2 affect the nature of the roots of (21). Since H_1 and H_2 are functions of the dependent variables, no *a priori* conclusion can be drawn.

Since the material is expected to dilate as it flows down the hopper, the above discussion suggests that the frictional–kinetic equations for hopper flow (with $\epsilon \ll 1$) are likely to be elliptic-hyperbolic in character.

With this knowledge of the structure of the governing equations, boundary conditions can now be specified.

2.3. *Boundary conditions*

Let us examine the governing equations (4)–(18) to determine the number of boundary conditions that are to be specified. The highest spatial derivatives in these equations are of first order with respect to v, and of second order with respect to U, V, and T'. This follows on using the coaxiality condition (15) and the flow rule (16) to express γ' and $\sin v_d$ in terms of the first derivatives of U and V. Then in view of (15), (16) and (18), the frictional stress gradients in (5) and (6) involve second derivatives of U and V. Similarly, the kinetic stress gradients involve second derivatives of U and V. Hence (4)–(18) must be supplemented in each of the X- and Y-directions by two conditions for U, V and T', and one condition for v. If v is regarded as a known function of position, the equations excluding the mass balance are likely to be elliptic (§ 2.2). Therefore, it is desirable to specify conditions along all boundaries of the flow domain. Earlier models for hopper flow have considered only the region within the hopper for analysis, with one boundary as the exit slot. However, since the nature of flow in the exit region is still poorly understood, it is very difficult to prescribe conditions for U, V, and T' along the exit slot. Hence the jet is included in

the analysis, and plausible downstream conditions are specified some distance below the exit.

2.3.1. *Upstream conditions*

It is convenient to choose the upstream boundary as the horizontal line $Y = Y_a$ (figure 1). The value of Y_a is chosen as follows. It is assumed that the height of material in the hopper is maintained approximately constant at $Y = H$ by feeding material at the top. Consider a 'deep' hopper with $H \gg Y_a \gg 1$. For such a hopper, numerical integration of the compressible frictional equations suggests that the stress and velocity fields converge to certain asymptotic fields as Y decreases (Prakash & Rao 1988, 1991). Even though this result has not been rigorously established, we shall use the asymptotic fields as a convenient means of specifying upstream conditions. Thus

$$v = v_a(X); \quad U = U_a(X); \quad V = V_a(X); \quad T' = T'_a(X) \ \text{ at } Y = Y_a, \tag{22}$$

where the functions v_a, U_a, V_a, and T'_a denote the asymptotic fields. Near the exit, inertial terms cause the actual fields to deviate from the asymptotic fields. Therefore Y_a is chosen so that at $Y = Y_a$ the inertial terms are small compared to the frictional stress gradients. At this value of Y, the kinetic stress gradients are also expected to be small. This conjecture is based on the incompressible results of Jyotsna & Rao (1991), which suggest that significant kinetic stress gradients occur only near the exit slot. The specific values of Y_a used will be indicated later.

The asymptotic fields v_a, U_a, and V_a in (22) are approximated using a perturbation solution due to Prakash & Rao (1991). This solution involves the numerical integration of certain ordinary differential equations. To simplify the analysis, we invoke the radial gravity assumption, thereby obtaining explicit expressions for the asymptotic fields (see Appendix A). The asymptotic temperature field T'_a is constructed as indicated below.

Considering the smooth-wall radial-gravity problem and using the asymptotic fields for U, V, and v, the conduction-free energy balance is integrated downwards. It is then found that, if integration is started high above the hopper exit, irrespective of the initial temperature specified, an asymptotic solution is attained as Y decreases (figure 15). Therefore, it is convenient to choose the asymptotic field value $T'_a(Y_a)$ as the upstream value of T'.

The downstream boundary conditions will now be specified.

2.3.2. *Downstream conditions*

These will be specified along a horizontal line $Y = Y_l < 0$ (figure 1). It is assumed that the velocity field at Y_l corresponds to vertical free-fall, i.e.

$$U = 0; \quad V \frac{\partial V}{\partial Y} + 1 = 0 \ \text{ at } \ Y = Y_l. \tag{23}$$

In the particle jet below the hopper, density profiles based on (23) (Fickie *et al.* 1989; Prakash & Rao 1991) show reasonable agreement with the measurements of Fickie *et al.* (1989). The downstream condition for T' is obtained by substituting (23) into the energy balance (7) and omitting the terms involving the heat flux. To simplify the subsequent analysis, it is assumed that $\frac{1}{2}(\partial U/\partial Y + \partial V/\partial X)^2$ is small compared to $(\partial V/\partial Y)^2$. This assumption holds along the centreline $X = 0$ in view of the boundary conditions $U = 0, \partial V/\partial X = 0$ at $X = 0$. At other locations, it is difficult to justify the

assumption *a priori*. Thus the downstream condition for T' is

$$\frac{3}{2}vV\frac{\partial T'}{\partial Y}-\frac{1}{V}\left[T'h_1+T'^{1/2}\,\frac{h_2'}{V}\right]+T'^{3/2}h_6=0 \quad \text{at} \quad Y=Y_l, \tag{24}$$

where the function h_2' is defined in table 1.

This completes the specification of the boundary conditions in the direction of flow. Additional boundary conditions must now be specified along the centreline, hopper wall, and free surface of the jet.

2.3.3. *Boundary conditions along the centreline*

For a symmetric solution, these are given by

$$U=0; \quad \frac{\partial V}{\partial X}=0; \quad \frac{\partial v}{\partial X}=0; \quad \frac{\partial T'}{\partial X}=0 \quad \text{at } X=0. \tag{25}$$

2.3.4. *Boundary conditions along the hopper wall and the free surface of the jet*

Along the smooth hopper wall, the normal component of velocity and the shear stress must vanish. Thus

$$U\cos\theta_w-V\sin\theta_w=0, \tag{26}$$

$$\tfrac{1}{2}(\sigma_{YY}-\sigma_{XX})\sin 2\theta_{\mathrm{w}}-\sigma_{XY}\cos 2\theta_w=0 \quad \text{at } X=X_*\,, Y\geqslant 0, \tag{27}$$

where $X_*=1+Y\tan\theta_w$ is the value of X along the hopper wall, and σ_{XX}, σ_{YY}, and σ_{XY} are given by (8).

Assuming that collisions between particles and the smooth wall are (i) specular and (ii) elastic, the boundary condition proposed by Johnson & Jackson (1987) implies that the flux of pseudo-thermal energy into the wall also vanishes, i.e.

$$\left(\sin\theta_w\frac{\partial T'}{\partial Y}-\cos\theta_w\frac{\partial T'}{\partial X}\right)=0 \quad \text{at} \quad X=X_*, Y\geqslant 0. \tag{28}$$

If assumption (ii) above is relaxed, the energy flux at the hopper wall will in general be non-zero, whereas the flux across the free surface of the jet must vanish. Anticipating that this may cause computational difficulties, we have considered the simpler case of elastic particle–wall collisions.

Along the free surface of the jet ($X=X_*$, $Y<0$), the normal component of velocity and the shear and normal stresses must vanish. Thus

$$U\cos\theta_*-V\sin\theta_*=0, \tag{29}$$

$$\tfrac{1}{2}(\sigma_{YY}-\sigma_{XX})\sin 2\theta_*-\sigma_{XY}\cos 2\theta_*=0, \tag{30}$$

$$\tfrac{1}{2}(\sigma_{XX}+\sigma_{YY})+\tfrac{1}{2}(\sigma_{XX}-\sigma_{YY})\cos 2\theta_*-\sigma_{XY}\sin 2\theta_*=0 \tag{31}$$

at $X=X_*, Y<0$, where σ_{XX}, σ_{YY} and σ_{XY} are given by (8), and θ_* is the inclination of the free surface to the vertical (figure 1). Equations (29)–(31) provide boundary conditions for U and V, and also serve to determine θ_*. The half-width of the jet X_* is given by

$$\frac{\mathrm{d}X_*}{\mathrm{d}Y}=\tan\theta_*, \quad Y<0. \tag{32}$$

There are practical difficulties in using (31) immediately below the hopper exit.

This is because, just above the exit, the normal stress on the hopper wall is in general non-zero. Therefore (31) implies a jump in normal stress at the edge of the exit slot. To overcome computational difficulties in this region, (31) is modified to

$$\tfrac{1}{2}(\sigma_{XX}+\sigma_{YY})+\tfrac{1}{2}(\sigma_{XX}-\sigma_{YY})\cos 2\theta_* - \sigma_{XY}\sin 2\theta_* = \sigma_{n0}\mathrm{e}^{k'Y} \quad \text{at } X = X_*,\ Y<0, \tag{33}$$

as suggested by V. H. Arakeri (1991, private communication). Here σ_{n0} is the normal stress on the wall, evaluated at the exit edge ($X=1, Y=0^+$) and k' is a positive constant. The value of k' is chosen so that the normal stress along the free surface is effectively zero at a distance of a few particle diameters below the exit.

Finally, the flux of pseudo-thermal energy across the free surface must vanish:

$$\sin\theta_*\frac{\partial T'}{\partial Y} - \cos\theta_*\frac{\partial T'}{\partial X} = 0 \quad \text{at } X = X_*,\ Y<0. \tag{34}$$

This completes the specification of boundary conditions for the two-dimensional problem. We now turn to the formulation of the quasi-one-dimensional model using the two-dimensional equations. This approximation is attempted because preliminary attempts to solve the latter equations numerically were unsuccessful.

3. Problem formulation for the quasi-one-dimensional model

3.1. *Governing equations*

Following the approach used in gas dynamics (Schreier 1982, pp. 33–37), the equations for the quasi-one-dimensional model are obtained by integrating the balance equations in the X-direction. Here it is convenient to use a coordinate transformation that maps the flow domain onto a rectangle. One choice is $\overline{X} = X/X_*(Y)$, $\overline{Y} = Y$ (see figure 1). Integrating (4) with respect to X from $X=0$ to $X = X_*(Y)$, and changing the independent variables to $(\overline{X},\overline{Y})$, we get

$$\frac{\mathrm{d}}{\mathrm{d}\overline{Y}}[X_*\langle vV\rangle] + v_*(U_* - V_*\tan\theta_*) = 0, \tag{35}$$

where the star denotes quantities evaluated at $\overline{X}=1$, and

$$\langle F\rangle \equiv \int_0^1 F(\overline{X},\overline{Y})\mathrm{d}\overline{X}$$

is the cross-sectional average of any quantity F.

Similarly, the momentum balances (5) and (6) may be written as

$$\frac{\mathrm{d}}{\mathrm{d}\overline{Y}}\left[X_*\langle vUV+\sigma_{XY}\rangle\right] - \sigma_{XX}|_{\overline{X}=0} + v_*U_*(U_*-V_*\tan\theta_*) + \sigma_{XX_*} - \sigma_{XY_*}\tan\theta_* = 0, \tag{36}$$

$$\frac{\mathrm{d}}{\mathrm{d}\overline{Y}}\left[X_*\langle vVV+\sigma_{YY}\rangle\right] + X_*\langle v\rangle + v_*V_*(U_*-V_*\tan\theta_*) + \sigma_{XY_*} - \sigma_{YY_*}\tan\theta_* = 0, \tag{37}$$

where σ_{XX}, σ_{YY}, and σ_{XY} are given by (8). Finally, the pseudo-thermal energy balance (7) takes the form

$$\frac{\mathrm{d}}{\mathrm{d}\overline{Y}}\left[X_*\langle \tfrac{3}{2}vVT'+q_Y\rangle\right] + X_*\langle H\rangle + \tfrac{3}{2}v_*T'_*(U_*-V_*\tan\theta_*) + q_{X_*} - q_{Y_*}\tan\theta_* = 0, \tag{38}$$

where q_X and q_Y are given by (10) and

$$H = \left(\frac{1}{X_*}\frac{\partial U}{\partial \overline{X}} + \frac{\partial V}{\partial \overline{Y}} - \frac{\overline{X}}{X_*}\tan\theta_*\frac{\partial V}{\partial \overline{X}}\right) \times \left[T'h_1 - T'^{1/2}\,\overline{h}_2\left(\frac{1}{X_*}\frac{\partial U}{\partial \overline{X}} + \frac{\partial V}{\partial \overline{Y}} - \frac{\overline{X}}{X_*}\tan\theta_*\frac{\partial V}{\partial \overline{X}}\right)\right] - 2T'^{1/2}h_3\left[\left(\frac{1}{X_*}\frac{\partial U}{\partial \overline{X}}\right)^2 + \left(\frac{\partial V}{\partial \overline{Y}} - \frac{\overline{X}}{X_*}\tan\theta_*\frac{\partial V}{\partial \overline{X}}\right)^2 + \frac{1}{2}\left(\frac{\partial U}{\partial \overline{Y}} - \frac{\overline{X}}{X_*}\tan\theta_*\frac{\partial U}{\partial \overline{X}} + \frac{1}{X_*}\frac{\partial V}{\partial \overline{X}}\right)^2\right] + T'^{3/2}h_6. \tag{39}$$

Equations (35)–(38) are simplified by using the boundary conditions (25)–(34). Thus, two sets of equations are obtained, one valid in the hopper ($\overline{Y} \geqslant 0$), and the other in the jet ($\overline{Y} < 0$). Considering the hopper, and using the boundary conditions, the balance equations reduce to

$$\frac{\mathrm{d}}{\mathrm{d}\overline{Y}}[X_*\langle vV\rangle] = 0, \tag{40}$$

$$\frac{\mathrm{d}}{\mathrm{d}\overline{Y}}\left[X_*\langle vUV + \sigma_{XY}\rangle\right] - \sigma_{XX}|_{\overline{X}=0} + \frac{\sigma_{XX_*} - \sigma_{YY_*}\tan^2\theta_w}{1-\tan^2\theta_w} = 0, \tag{41}$$

$$\frac{\mathrm{d}}{\mathrm{d}\overline{Y}}\left[X_*\langle vVV + \sigma_{YY}\rangle\right] + X_* < v > + \tan\theta_w\frac{\sigma_{YY_*}\tan^2\theta_w - \sigma_{XX_*}}{1-\tan^2\theta_w} = 0, \tag{42}$$

$$\frac{\mathrm{d}}{\mathrm{d}\overline{Y}}\left[X_*\langle \tfrac{3}{2}vVT' + q_Y\rangle\right] + X_*\langle H\rangle = 0, \tag{43}$$

where $\theta_* = \theta_w$ and $X_* = 1 + \overline{Y}\tan\theta_w$. These must be supplemented by (8)–(18).

The corresponding equations for the jet are (40)–(43) (with θ_w replaced by θ_*), and

$$(\sigma_{XX_*} + \sigma_{YY_*}) + (\sigma_{XX_*} - \sigma_{YY_*})\sec 2\theta_* - 2\sigma_{n0}\mathrm{e}^{k'\overline{Y}} = 0, \tag{44}$$

$$\frac{\mathrm{d}X_*}{\mathrm{d}\overline{Y}} - \tan\theta_* = 0 \quad \text{or} \quad \frac{\mathrm{d}X_*}{\mathrm{d}\overline{Y}} - \frac{U_*}{V_*} = 0, \tag{45}$$

together with (8)–(18). In (45), $U_* = U(\overline{X}=1,\overline{Y})$ and $V_* = V(\overline{X}=1,\overline{Y})$.

To proceed further, suitable transverse profiles must be chosen for the variables. Here it is assumed that the hopper walls are steep, i.e. the wall angle θ_w (figure 1) is $\ll 1$. In this limit, we assume that $\tan\theta_* \simeq \theta_*$, $\sin 2\theta_* \simeq 2\theta_*$, $\cos 2\theta_* \simeq 1$, and omit the terms involving $\tan^2\theta_w$ in (41) and (42). The following expressions are assumed for the dependent variables :

$$\left.\begin{aligned} v &= v\,(\overline{Y}),\\ U &= (4\langle U\rangle - V\theta_*)\,(\overline{X} - \overline{X}^3) + V\theta_*\overline{X}^3,\\ V &= V\,(\overline{Y}),\\ T' &= T'\,(\overline{Y}). \end{aligned}\right\} \tag{46}$$

Here $\langle U\rangle$ denotes the cross-sectional averaged value of the X-component of velocity. The profile for U satisfies the condition of zero normal velocity at $\overline{X} = 0$ and $\overline{X} = 1$. Owing to the simple expressions assumed, the boundary conditions (27), (28),

(30), and (34) are not satisfied exactly. For example, using (46), the left-hand side of (28) reduces to $\sin\theta_w(\mathrm{d}T'/\mathrm{d}\overline{Y})$, which is non-zero in general. However, the error incurred may not be large, as our analysis is restricted to small values of θ_w. The boundary conditions can be satisfied more accurately by including $\overline{X}$-dependence for the variables v, V, and T', but this results in a larger system of coupled equations. We shall see that even the present system of equations poses considerable numerical difficulties.

At this stage, two other modifications in the model must be explained.

(*a*) Equations (46) and the coaxiality condition (15) imply that $\gamma' = \theta_*/2$ along the hopper wall and free surface of the jet. This is exactly half the value required for the shear stress to vanish at the boundary. To overcome this difficulty while retaining the simple forms for the variables, the approximation $\gamma' = \theta_*\overline{X}$ is used instead of (15). This choice is consistent with the requirement that γ' be an odd function of $\overline{X}$ (for a symmetric solution), and it also ensures that the shear stress vanishes along $\overline{X} = 0$ and $\overline{X} = 1$.

(*b*) For the materials considered in the present work, $n - 1 \ll 1$. Therefore (18) implies that $\mathrm{d}\alpha/\mathrm{d}\sin v_d \to \infty$ as $\sin v_d \to n\sin\phi$, i.e. as $\alpha \to 0$. This may cause computational difficulties when $\alpha \to 0$. To avoid problems in this region, the steep part of the relation between α and $\sin v_d$ is replaced by a cubic fit, so that $\mathrm{d}\alpha/\mathrm{d}\sin v_d = 0$ at the maximum value of $\sin v_d$. As a result of this modification, α is determined from the equations

$$\alpha = \begin{cases} (1-\delta)^{(n-1)}; & \delta \equiv \dfrac{\sin v_d}{n\sin\phi} \leqslant \delta_1 \\ (\delta-\delta_2)^2\,(a_1(\delta-\delta_2)+a_2); & \delta_1 < \delta < \delta_2 \\ 0; & \delta \geqslant \delta_2, \end{cases} \tag{47}$$

with $\delta_1 = 0.98$ and $\delta_2 = 1.1$, and a_1 and a_2 are constants. The upper limit of δ is chosen as 1.1 to reduce the steepness of the cubic fit. It is not clear if such an extension is justified, but it is used here to avoid undue numerical difficulties.

With profiles (46) and the above modifications, the equations in the hopper ($\overline{Y} \geqslant 0$) reduce to:

mass balance

$$X_* v V = \text{constant} \equiv c_1. \tag{48}$$

Here c_1 is related to the mass flow rate $\dot{M}$ by

$$c_1 = \frac{-\dot{M}}{2\rho_p w B'(gw)^{1/2}},$$

where B' is the width of the hopper in the direction perpendicular to the plane of figure 1;

momentum balance (X-component)

$$\frac{\mathrm{d}}{\mathrm{d}\overline{Y}}\left\{c_1\langle U\rangle - X_*\langle 2\tau'\theta_w\overline{X}\rangle - \epsilon T'^{1/2}h_3\left[X_*\frac{\mathrm{d}\langle U\rangle}{\mathrm{d}\overline{Y}} + \theta_w(\langle U\rangle - U_*)\right]\right\}$$
$$+(\sigma'+\tau')|_{\overline{X}=1} - (\sigma'+\tau')|_{\overline{X}=0} + \epsilon T'^{1/2}\left[\frac{6h_2'}{X_*}(2\langle U\rangle - U_*)\right] = 0, \tag{49}$$

momentum balance (Y-component)

$$\frac{\mathrm{d}}{\mathrm{d}\overline{Y}}\left\{c_1V+X_*(\langle\sigma'-\tau'\rangle+\epsilon T'h_1)-\epsilon T'^{1/2}\left(\overline{h}_2U_*+X_*h_2'\frac{\mathrm{d}V}{\mathrm{d}\overline{Y}}\right)\right\}+\frac{c_1}{V}$$
$$-\theta_w\left[(\sigma'+\tau')|_{\overline{X}=1}+\epsilon T'h_1+\epsilon T'^{1/2}\left(\frac{h_2'}{X_*}(8\langle U\rangle-5U_*)-\overline{h}_2\frac{\mathrm{d}V}{\mathrm{d}\overline{Y}}\right)\right]=0, \quad (50)$$

pseudo-thermal energy balance

$$\frac{\mathrm{d}}{\mathrm{d}\overline{Y}}\left\{\tfrac{3}{2}c_1T'-\epsilon T'^{1/2}h_4X_*\frac{\mathrm{d}T'}{\mathrm{d}\overline{Y}}\right\}+X_*\left\{T'h_1\left(\frac{\mathrm{d}V}{\mathrm{d}\overline{Y}}+\frac{U_*}{X_*}\right)-2T'^{1/2}\overline{h}_2\frac{U_*}{X_*}\frac{\mathrm{d}V}{\mathrm{d}\overline{Y}}\right.$$
$$-T'^{1/2}h_2'\left[\left(\frac{\mathrm{d}V}{\mathrm{d}\overline{Y}}\right)^2+\frac{64\langle U\rangle(\langle U\rangle-U_*)+21U_*^2}{5X_*^2}\right]$$
$$-T'^{1/2}h_3\left[\frac{1}{3}\left(4\frac{\mathrm{d}\langle U\rangle}{\mathrm{d}\overline{Y}}-\frac{\mathrm{d}U_*}{\mathrm{d}\overline{Y}}-\frac{\theta_w}{X_*}(4\langle U\rangle-U_*)\right)^2\right.$$
$$+\frac{8}{35}\left(\frac{\mathrm{d}U_*}{\mathrm{d}\overline{Y}}-2\frac{\mathrm{d}\langle U\rangle}{\mathrm{d}\overline{Y}}+\frac{3\theta_w}{X_*}(2\langle U\rangle-U_*)\right)\left(9\frac{\mathrm{d}\langle U\rangle}{\mathrm{d}\overline{Y}}-\frac{\mathrm{d}U_*}{\mathrm{d}\overline{Y}}\right.$$
$$\left.\left.\left.+\frac{\theta_w}{X_*}(\langle U\rangle-4U_*)\right)\right]+T'^{3/2}h_6\right\}=0, \quad (51)$$

where $U_*=V\theta_w$. Using (46) and (16) (with $\cos 2\gamma'=\cos(2\theta_w\overline{X})\simeq 1$), we get

$$\sin v_d=\frac{X_*\mathrm{d}V/\mathrm{d}\overline{Y}+4\langle U\rangle-U_*-6\overline{X}^2(2\langle U\rangle-U_*)}{X_*\mathrm{d}V/\mathrm{d}\overline{Y}-4\langle U\rangle+U_*+6\overline{X}^2(2\langle U\rangle-U_*)}. \quad (52)$$

The frictional stresses in the momentum balances (49) and (50) are evaluated using (11), (13), (14), (47), and (52).

The equations in the jet ($\overline{Y}<0$) take the forms:

momentum balance (X-component)

$$\frac{\mathrm{d}}{\mathrm{d}\overline{Y}}\left\{c_1\langle U\rangle-X_*\langle 2\tau'\theta_*\overline{X}\rangle-\epsilon T'^{1/2}h_3\left[X_*\frac{\mathrm{d}\langle U\rangle}{\mathrm{d}\overline{Y}}+\theta_*(\langle U\rangle-U_*)\right]\right\}$$
$$+\sigma_{n0}e^{k'\overline{Y}}-(\sigma'+\tau')|_{\overline{X}=0}-\epsilon T'h_1+\epsilon T'^{1/2}\left[\overline{h}_2\frac{\mathrm{d}V}{\mathrm{d}\overline{Y}}+\frac{h_2'}{X_*}(4\langle U\rangle-U_*)\right]=0, \quad (53)$$

momentum balance (Y-component)

$$\frac{\mathrm{d}}{\mathrm{d}\overline{Y}}\left\{c_1V+X_*(\langle\sigma'-\tau'\rangle+\epsilon T'h_1)-\epsilon T'^{1/2}\left(\overline{h}_2U_*+X_*h_2'\frac{\mathrm{d}V}{\mathrm{d}\overline{Y}}\right)\right\}$$
$$+\frac{c_1}{V}-\theta_*\sigma_{n0}\mathrm{e}^{k'\overline{Y}}=0, \quad (54)$$

where $U_*=V\theta_*$ and σ' and τ' are given by (11), (13), (14), (47), and (52) (with θ_w replaced by θ_*). The normal stress condition (44) reduces to $\sigma_{XX*}\simeq\sigma_{n0}\mathrm{e}^{k'\overline{Y}}$, or

$$(\sigma'+\tau')|_{\overline{X}=1}+\epsilon T'h_1-\epsilon T'^{1/2}\left[\overline{h}_2\frac{\mathrm{d}V}{\mathrm{d}\overline{Y}}+\frac{h_2'}{X_*}(5U_*-8\langle U\rangle)\right]-\sigma_{n0}\mathrm{e}^{k'\overline{Y}}=0, \quad (55)$$

while the mass and energy balances, and the equation for X_* are given by (48), (51) (with θ_w replaced by θ_*), and (45), respectively.

For a specified value of c_1, the variables to be solved for are $\langle U\rangle$, V, and T' in the hopper, and $\langle U\rangle$, V, T', U_*, and X_* in the jet. The solids fraction v is determined using (48), and the final value of c_1 is chosen as explained in § 6.1. To solve the above equations, we must specify boundary conditions in the $\overline{Y}$-direction.

3.2. *Boundary conditions*

The boundary conditions in the $\overline{Y}$-direction are given by the averaged counterparts of the conditions discussed in § 2.3. Therefore, at the upstream end $\overline{Y} = \overline{Y}_a$, the values of $\langle U\rangle$, V and T' are prescribed using the averaged asymptotic fields for the compressible SWRG problem. Using the small angle approximation, the upstream velocity conditions may be written as

$$\langle U\rangle = v'\theta_w/2; \quad V = v' \quad \text{at } \overline{Y} = \overline{Y}_a, \tag{56}$$

where v' is the dimensionless radial velocity given by (A1). In (A1), $\xi' \simeq \overline{Y} + (1/\theta_w)$ is the dimensionless radial coordinate.

The downstream boundary conditions are obtained by integrating (23) and (24) with repect to $\overline{X}$, from $\overline{X} = 0$ to $\overline{X} = 1$, and using the profiles (46). The result is

$$\langle U\rangle = 0; \quad V\frac{\mathrm{d}V}{\mathrm{d}Y} + 1 = 0; \quad \text{at } \overline{Y} = \overline{Y}_l, \tag{57}$$

$$\frac{3}{2}c_1\frac{\mathrm{d}T'}{\mathrm{d}\overline{Y}} - X_*\left(\frac{T'h_1}{V} + \frac{T'^{1/2}h_2'}{V^2} - T'^{3/2}h_6\right) = 0 \quad \text{at } \overline{Y} = \overline{Y}_l. \tag{58}$$

This completes the formulation of the quasi-one-dimensional approximation. Before considering the solution procedure, let us briefly discuss the work of Hankey & Thomas (1991). This is based on a quasi-one-dimensional model for unsteady flow. It differs from the present work in the following respects: (i) kinetic effects are omitted, (ii) only the mass balance and the Y-component of the momentum balance are solved, (iii) the normal stress σ_{YY} is assumed to be a known function of the density, and (iv) the free surface of the jet is assumed to be vertical. The present work attempts to relax some of these constraints. In the process, many difficulties arise, as explained shortly.

4. Solution strategy for the quasi-one-dimensional equations

It is useful to divide the flow domain into two regions, as indicated in figure 1. In the upper region ($\overline{Y}_a \geqslant \overline{Y} \geqslant \overline{Y}_u$), frictional effects dominate, as is evident from the incompressible results (Jyotsna & Rao 1991), and also the compressible results presented later (figure 8). In the lower region ($\overline{Y}_u > \overline{Y} \geqslant \overline{Y}_l$), both frictional and kinetic effects are expected to be comparable. The present work is based on a different numerical scheme for each region, as the use of a single scheme for both the regions did not give satisfactory results.

In the upper region, an initial-value approach is used to solve the frictional limit of (48)–(50), obtained by omitting the terms containing ϵ in the momentum balances. The averaged SWRG asymptotic fields (56) are used as initial conditions. An additional initial condition is required for V, since (11)–(13), (47) and (52) imply that (49) and (50) involve the second derivative of V. This condition is provided by prescription of the slope $\mathrm{d}V/\mathrm{d}\overline{Y}$ at $\overline{Y} = \overline{Y}_a$. As seen later, the solution is found to be relatively insensitive to the value used for $\mathrm{d}V/\mathrm{d}\bar{Y}$ ($\overline{Y}_a$).

Consider downward integration of the frictional equations, using the initial conditions discussed above. The integration breaks down as the mean stress at a critical state (σ_c') tends to zero. This is because the coefficient of the highest derivative of V in (49) and (50) is proportional to σ_c'. In practice, small values of σ_c' result in a sharp increase in the gradients of all the variables. Therefore, downward integration is terminated at a value $\overline{Y} = \overline{Y}_u$. The values of $\overline{Y}_u$ and the constant c_1, which is proportional to the mass flow rate, are chosen as described later. A suitable choice of c_1 ensures that the lower frictional–kinetic region $\overline{Y}_u > \overline{Y} \geqslant \overline{Y}_l$ spans the exit slot when $\overline{Y}_l$ is chosen to be < 0. It must also be mentioned that the conduction-free energy balance is solved as part of the initial-value problem, to obtain the temperature at $\overline{Y}_u$, the upstream boundary of the lower region. The initial condition used for the energy balance is obtained from the SWRG asymptotic temperature field, as discussed in Appendix A.

Initially the finite element method was chosen to solve the equations in both the regions. An attempt was made to solve the resulting system of nonlinear equations using the Newton–Raphson method. Unfortunately, in spite of a large variety of initial fields used, the iterations for the frictional–kinetic equations failed to converge. Therefore, in order to avoid iteration, the equations for the lower region were linearized about a suitable state, and a semi-analytical solution was constructed. It is hoped that this solution may provide suitable initial fields for future attempts to solve the nonlinear problem. The finite element formulation in the first region is retained, since integration of the frictional equations poses no difficulties for small wall angles.

Let us now consider the details of the methods used to solve the equations in the two regions. We start with the finite element method for the initial-value frictional problem, given by (48)–(51) with $\epsilon = 0$. As noted earlier, the solution of (51) provides an upstream condition for T', to be used when the equations for the lower region are integrated.

4.1. *Finite element method for the initial-value problem*

In the upper region $\overline{Y}_a \geqslant \overline{Y} \geqslant \overline{Y}_u$, a one-dimensional finite element method (Zienkiewicz 1977, pp. 570–572, 581–584) is used to solve the initial-value problem. Quadratic basis functions are used for the vertical velocity V. Since only first derivatives of $\langle U \rangle$ and T' occur in the governing equations, linear basis functions are used for these variables. Weighted residuals are formed using the sub-domain method (Zienkiewicz 1977, pp. 50, 587), which is a popular scheme for initial-value problems. The resulting nonlinear equations are solved using the Newton–Raphson method with the elements of the Jacobian matrix approximated by a centred difference scheme.

Let us now consider the solution procedure for the lower region.

4.2. *Linearization of the equations*

The following approximations are used to simplify the equations in the region $\overline{Y} < \overline{Y}_u$:

(i) The viscosities $\epsilon T'^{1/2} h_2$, $\epsilon T'^{1/2} h_3$ and the thermal conductivity $\epsilon T'^{1/2} h_4$ are treated as constants.

(ii) The frictional variables $\bar{\alpha} \equiv \langle \alpha \rangle$, $\alpha_0 \equiv \alpha(\overline{X} = 0, \overline{Y})$, $\alpha_1 \equiv \alpha(\overline{X} = 1, \overline{Y})$, $\bar{f} \equiv \langle f(\alpha) \rangle$, $f_0 \equiv f(\alpha_0)$, $f_1 \equiv f(\alpha_1)$, and $f_2 \equiv \langle 2f(\alpha)\overline{X} \rangle$, are replaced by their values at $\overline{Y}_u^+$. Here α is as defined in (11), and the angular brackets denote cross-sectional averages.

(iii) The coefficients of the Y-derivatives of the velocities $\langle U \rangle$, U_*, and V, the temperature T', and the solids fraction ν are treated as constants, even when they involve $\mathrm{d}X_*/\mathrm{d}\overline{Y}$ $(= \theta_*)$.

(iv) Nonlinear terms such as $\left(\mathrm{d}V/\mathrm{d}\overline{Y}\right)^2$, $\sigma_c'(v)$, and U_*/X_* are linearized about their values at $\overline{Y} = \overline{Y}_u^+$. However terms involving $\mathrm{d}X_*/\mathrm{d}\overline{Y}$, but not the derivatives of velocities and the temperature, are simplified before linearization.

(v) In the jet, $\mathrm{d}X_*/\mathrm{d}\overline{Y}$ is replaced by $\theta_* = U_*/V$ (see (45)) before linearization.

(vi) All constants are evaluated at $\overline{Y} = \overline{Y}_u^+$. Since $\overline{Y}_u > 0$ and the equations in the jet are valid only for $\overline{Y}_l < \overline{Y} < 0$, this is reasonable only if both $\overline{Y}_u$ and $\overline{Y}_l$ are close to 0.

(vii) In the term $\theta_*\sigma_{n0}\mathrm{e}^{k'\overline{Y}}$, which occurs in (54), θ_* is approximated by θ_w.

Using (i)–(vii), the linearized versions of (49)–(51) are given by

$$a_{11}\frac{\mathrm{d}^2\langle U\rangle}{\mathrm{d}\overline{Y}^2} + a_{12}\frac{\mathrm{d}\langle U\rangle}{\mathrm{d}\overline{Y}} + a_{13}\frac{\mathrm{d}V}{\mathrm{d}\overline{Y}} + a_{14}\langle U\rangle + a_{15}V + a_{16}X_* + a_{17} = 0, \tag{59}$$

$$b_{11}\frac{\mathrm{d}^2V}{\mathrm{d}\overline{Y}^2} + b_{12}\frac{\mathrm{d}V}{\mathrm{d}\overline{Y}} + b_{13}\frac{\mathrm{d}T'}{\mathrm{d}\overline{Y}} + b_{14}\langle U\rangle + b_{15}V + b_{16}T' + b_{17}X_* + b_{18} = 0, \tag{60}$$

$$c_{11}\frac{\mathrm{d}^2T'}{\mathrm{d}\overline{Y}^2} + c_{12}\frac{\mathrm{d}T'}{\mathrm{d}\overline{Y}} + c_{13}\frac{\mathrm{d}\langle U\rangle}{\mathrm{d}\overline{Y}} + c_{14}\frac{\mathrm{d}V}{\mathrm{d}\overline{Y}} + c_{15}\langle U\rangle + c_{16}V + c_{17}T' + c_{18}X_* + c_{19} = 0, \tag{61}$$

where the coefficients a_{1j}–c_{1j} are defined in Appendix B.†

In the jet, the linearized versions of (53), (54), (51) (with θ_w replaced by θ_*), (55), and (45) are given by

$$g_{21}\frac{\mathrm{d}^2\langle U\rangle}{\mathrm{d}\overline{Y}^2} + g_{22}\frac{\mathrm{d}^2V}{\mathrm{d}\overline{Y}^2} + g_{23}\frac{\mathrm{d}\langle U\rangle}{\mathrm{d}\overline{Y}} + g_{24}\frac{\mathrm{d}V}{\mathrm{d}\overline{Y}} + g_{25}\frac{\mathrm{d}T'}{\mathrm{d}\overline{Y}} + g_{26}\frac{\mathrm{d}X_*}{\mathrm{d}\overline{Y}} + g_{27}\langle U\rangle + g_{28}V + g_{29}T' + g_{20}X_* + h_{21}\sigma_{n0}\mathrm{e}^{k'\overline{Y}} + h_{22} = 0, \tag{62}$$

$$l_{21}\frac{\mathrm{d}^2V}{\mathrm{d}\overline{Y}^2} + l_{22}\frac{\mathrm{d}\langle U\rangle}{\mathrm{d}\overline{Y}} + l_{23}\frac{\mathrm{d}V}{\mathrm{d}\overline{Y}} + l_{24}\frac{\mathrm{d}T'}{\mathrm{d}\overline{Y}} + l_{25}\frac{\mathrm{d}X_*}{\mathrm{d}\overline{Y}} + l_{26}\langle U\rangle + l_{27}V + l_{28}T' + l_{29}X_* + l_{20}\sigma_{n0}\mathrm{e}^{k'\overline{Y}} + h_{23} = 0, \tag{63}$$

$$m_{21}\frac{\mathrm{d}^2V}{\mathrm{d}\overline{Y}^2} + m_{22}\frac{\mathrm{d}^2T'}{\mathrm{d}\overline{Y}^2} + m_{23}\frac{\mathrm{d}\langle U\rangle}{\mathrm{d}\overline{Y}} + m_{24}\frac{\mathrm{d}V}{\mathrm{d}\overline{Y}} + m_{25}\frac{\mathrm{d}T'}{\mathrm{d}\overline{Y}} + m_{26}\frac{\mathrm{d}X_*}{\mathrm{d}\overline{Y}} + m_{27}\langle U\rangle + m_{28}V + m_{29}T' + m_{20}X_* + h_{24}\sigma_{n0}\mathrm{e}^{k'\overline{Y}} + h_{25} = 0, \tag{64}$$

$$d_{21}\frac{\mathrm{d}V}{\mathrm{d}\overline{Y}} + d_{22}\langle U\rangle + d_{23}V + d_{24}U_* + d_{25}T' + d_{26}X_* - \sigma_{n0}e^{k'\overline{Y}} + d_{27} = 0, \tag{65}$$

$$n_{21}\frac{\mathrm{d}V}{\mathrm{d}\overline{Y}} + \frac{\mathrm{d}X_*}{\mathrm{d}\overline{Y}} + n_{22}\langle U\rangle + n_{23}V + n_{24}T' + n_{25}X_* + n_{26}\sigma_{n0}e^{k'\overline{Y}} + n_{27} = 0, \tag{66}$$

where the coefficients $g_{2j} - n_{2j}$ are defined in table 2,† and the d_{2j} are defined in Appendix B†. It must be noted that (65) has been used to eliminate U_* and $\mathrm{d}U_*/\mathrm{d}\overline{Y}$ from (62)–(64) and (66).

Equations (59)–(66) are solved using specified values of $\langle U\rangle$, V and T' at the upstream boundary $\overline{Y} = \overline{Y}_u$, and the linearized versions of the downstream conditions

† Appendix B and table 2 are available on request from the authors or the Journal of Fluid Mechanics Editorial Office.

(57) and (58) at $\overline{Y} = \overline{Y}_l$. Values of the variables at $\overline{Y} = \overline{Y}_u$ are obtained from the solution of the initial-value problem, and may be written as

$$\langle U \rangle = \langle U \rangle_u; \quad V = V_u; \quad T' = T'_u \ \text{ at } \overline{Y} = \overline{Y}_u. \tag{67}$$

The downstream conditions are given by

$$\langle U \rangle = 0; \ \frac{\mathrm{d}V}{\mathrm{d}\overline{Y}} + p_{11}V + p_{12} = 0, \tag{68}$$

$$p_{21}\frac{\mathrm{d}T'}{\mathrm{d}\overline{Y}} + p_{22}V + p_{23}T' + p_{24}X_* + p_{25} = 0 \text{ at } \overline{Y} = \overline{Y}_l, \tag{69}$$

where the coefficients p_{ij} are defined in Appendix B†. All the coefficients in table 2 and Appendix B are evaluated using the upstream values of the variables at $\overline{Y} = \overline{Y}_u^+$. This completes the formulation of the linearized problem.

4.3. *Solution procedure used for the linearized boundary-value problem*

Introducing new variables defined by

$$\frac{\mathrm{d}\langle U \rangle}{\mathrm{d}\bar{Y}} = U_d; \quad \frac{\mathrm{d}V}{\mathrm{d}\bar{Y}} = V_d; \quad \frac{\mathrm{d}T'}{\mathrm{d}\bar{Y}} = T_d, \tag{70}$$

the equations in the hopper and the jet may be written in matrix form as

$$\frac{\mathrm{d}\boldsymbol{Z}_h}{\mathrm{d}\bar{Y}} = \boldsymbol{A}_h\, \boldsymbol{Z}_h + \boldsymbol{B}_h\, \bar{Y} + \boldsymbol{C}_h, \tag{71}$$

$$\frac{\mathrm{d}\boldsymbol{Z}_j}{\mathrm{d}\bar{Y}} = \boldsymbol{A}_j\, \boldsymbol{Z}_j + \boldsymbol{B}_j\, \sigma_{n0}\mathrm{e}^{k'\bar{Y}} + \boldsymbol{C}_j, \tag{72}$$

where

$$\boldsymbol{Z}_h{}^T = \left[\langle U \rangle,\ V,\ T',\ U_d,\ V_d,\ T_d\right], \tag{73}$$

$$\boldsymbol{Z}_j{}^T = \left[\langle U \rangle,\ V,\ T',\ X_*,\ U_d,\ V_d,\ T_d\right], \tag{74}$$

$\boldsymbol{A}_h$ and $\boldsymbol{A}_j$ are constant matrices, and $\boldsymbol{B}_h$, $\boldsymbol{C}_h$, $\boldsymbol{B}_j$ and $\boldsymbol{C}_j$ are constant vectors.

The forms of the non-homogeneous terms in (71) and (72) suggest simple particular solutions. These are then combined with the homogeneous solutions, the latter being expressed in terms of the eigenvalues and eigenvectors of $\boldsymbol{A}_h$ and $\boldsymbol{A}_j$. Finally, the boundary conditions (67)–(69) and the requirement of continuity of the variables at $\bar{Y} = 0$ suffice to determine the normal stress σ_{n0}, and the other constants occurring in the solution.

Real and distinct eigenvalues are obtained for the parameter values for Leighton Buzzard sand. In the case of glass beads, there is a pair of complex eigenvalues in both the hopper and the jet sections.

For a given set of parameter values, the solution is generated for different values of c_1. A starting guess for c_1 is obtained from an estimate of the discharge rate, described in Section C.3 of Prakash & Rao (1991). This estimate is modified as described later. Let us now consider the choice of parameter values.

5. Parameter values

Most of the results are presented for a material whose frictional properties correspond to Leighton Buzzard sand. Using the data of Airey, Budhu & Wood (1985),

† Appendix B and table 2 are available on request from the authors or the Journal of Fluid Mechanics Editorial Office.

the frictional parameters are found to be $\phi = 35^\circ, n = 1.03, \Gamma_1 = 1.81$, and $\lambda_1 = 0.025$. Unfortunately, the particle size distribution has not been reported in their paper. Blair-Fish & Bransby (1973) used Leighton Buzzard sand with a size range of 0.6–1.2 mm in their bunker experiments. Thus the data of Airey *et al.* (1985) probably represents the response of a material with a range of particle sizes. In the present model, the particle size occurs explicitly only in the kinetic constitutive equations. As the kinetic theory has not yet been developed for a polydisperse material, a nominal particle diameter of 1 mm is used here.

The solid density ρ_p is taken to be 2650 kg m^{-3} (J. R. Prakash 1992, private communication). The parameter β $(= p_a/\rho_p g w)$ is chosen as 590, which corresponds to a slot width $2w = 0.013$ m. The kinetic parameters are chosen as $\epsilon = (d_p/w)^2 = 0.024$ and $\eta = (1 + e_p)/2 = 0.9$, where e_p is the coefficient of restitution for interparticle collisions. This value of ϵ corresponds to a particle diameter $d_p = 1$ mm. The values of w and d_p match those used in the experiments of Fickie *et al.* (1989). The results for Leighton Buzzard sand correspond to a hopper wall angle $\theta_w = 5^0$.

For glass beads, the predicted solids fraction profile will be compared with the data of Fickie *et al.* (1989). Although their experiments were conducted with $\theta_w = 23^\circ$, this value causes computational difficulties, as discussed in the next section; therefore a smaller value of 5° is used. The parameter values corresponding to their data are $\phi = 32.4^\circ$ (R. Jackson 1989, private communication), $\Gamma_1 = 1.47, \lambda_1 = 0.049, \beta = 548, \rho_p = 2900$ kg m^{-3} and $\epsilon = 0.024$. Here Γ_1 and λ_1 are estimated using the data of Fickie *et al.* (1989), as discussed in § A.1.

Owing to the lack of relevant data for glass beads, the value of the parameter n in (13) is taken as 1.03, which is the value used for Leighton Buzzard sand. The value of $\eta = 0.9$ is also retained.

To complete the parameter specification, the value of the model parameter k' and details of the cubic fits used must be given. The value of k' in (33) is chosen as 10, so that the normal stress along the free surface decays to $\simeq 5\%$ of its value at the exit, over a distance of two particle diameters. The parameters σ_{c1} and σ_{c2} in (14) are for: (*a*) Leighton Buzzard sand: $v_1 = 0.52$, $v_{min} = 0.5$, $\sigma_{c1} = 7.67 \times 10^5$, $\sigma_{c2} = 663$, (*b*) glass beads: $v_1 = 0.52$, $v_{min} = 0.5$, $\sigma_{c1} = -3241$, $\sigma_{c2} = 197$. For $n = 1.03$, the parameters in (47) are $a_1 = 936.6$ and $a_2 = 174.1$.

6. Results

6.1. *Results for Leighton Buzzard sand*

Consider the frictional solution in the region $\overline{Y} \leqslant \overline{Y}_a$, for $c_1 = -2.77$. The reason for this choice of c_1 will be indicated later. In the lower part of the hopper, the velocity and temperature profiles are found to be insensitive to the values of $\bar{Y}_a$ and $V_{da} \equiv \mathrm{d}V/\mathrm{d}\bar{Y}$ $(\bar{Y} = \bar{Y}_a)$ (figure 2*a–c*). The approach to a common or asymptotic curve for different values of V_{da} is not visible on the scale of figure 2(*b*), since it occurs very close to $\overline{Y}_a$. On the other hand, the temperature profiles approach the asymptotic curve only around $\bar{Y} \simeq 10$ (figure 2*c*). Thus for $\bar{Y} < 10$, the frictional equations together with the conduction-free energy balance, behave effectively like a system of first-order equations, even though (49) and (50) involve the second derivative of V. Therefore, when the frictional–kinetic equations are solved in the lower region $\bar{Y}_u > \bar{Y} > \bar{Y}_l$ (figure 1), only the values of the variables can be matched at $\bar{Y} = \bar{Y}_u$. This results in discontinuities of derivatives such as $\mathrm{d}V/\mathrm{d}\bar{Y}$ at $\bar{Y}_u$. These discontinuities can be reduced by a suitable choice of $\bar{Y}_u$, as discussed below.

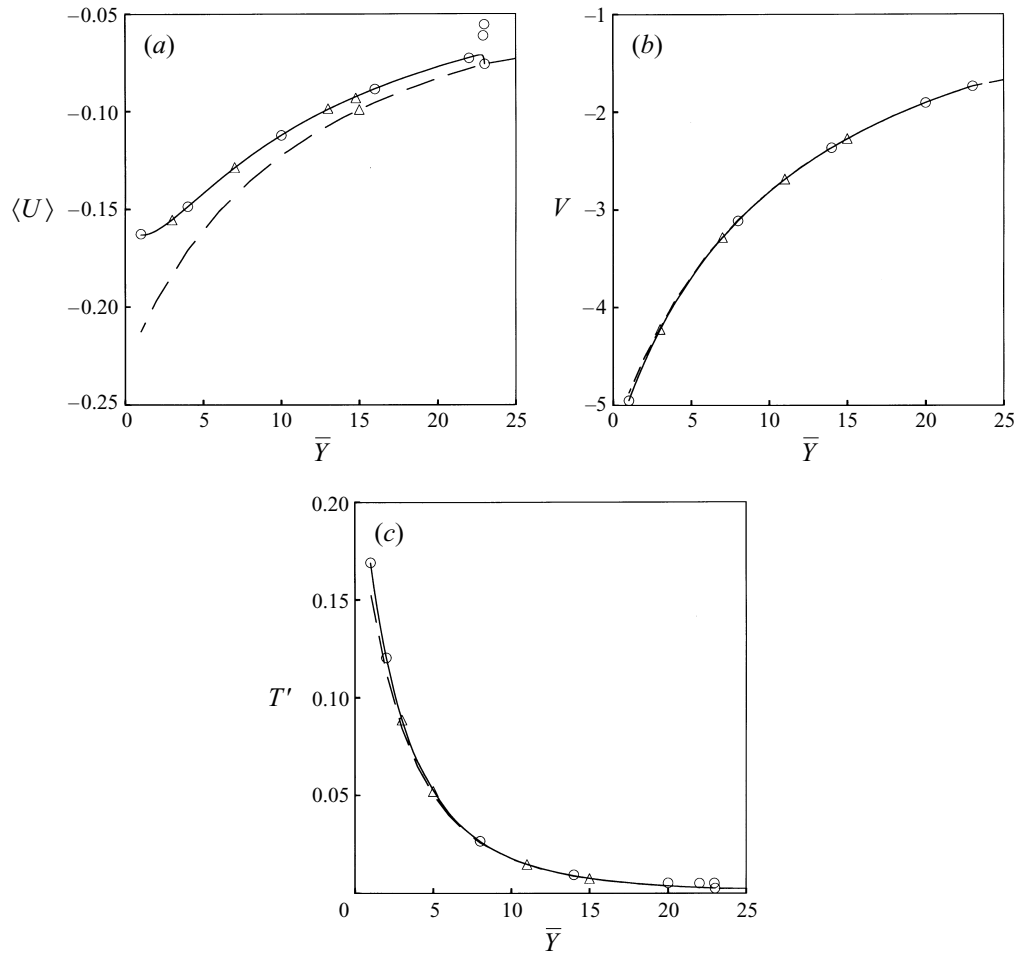

FIGURE 2. Effect of the values of $V_{da} \equiv \mathrm{d}V/\mathrm{d}\bar{Y}\,(\bar{Y} = \bar{Y}_a)$ and $\bar{Y}_a$ on the profile of (*a*) the average horizontal velocity, (*b*) the vertical velocity and (*c*) the temperature, for the upper region: - -, SWRG asymptotic field; —, ○, △, quasi-one-dimensional model (—, $\bar{Y}_a = 23$, $V_{da} = 0.05113$ (the SWRG value); ○, $\bar{Y}_a = 23$, $V_{da} = 0.1$; △, $\bar{Y}_a = 15$, $V_{da} = 0.08702$ (the SWRG value), $T'(\bar{Y}_a) = 0.002616$, 0.02616 and 0.007528 respectively in (*c*)). Parameter values: $\theta_w = 5°$, $\rho_p = 2650$ kg m^{-3}, $\beta = 590$, $\phi = 35°$, $\Gamma_1 = 1.81$, $\lambda_1 = 0.025$, $n = 1.03$, $v_1 = 0.52$, $v_{min} = 0.5$ and $c_1 = -2.77$.

Figures 2(*b*) and 2(*c*) show that the V and T' profiles are close to the asymptotic fields of the SWRG problem. This is reasonable since inertial terms are small except close to the exit, and radial gravity should be a good approximation for vertical gravity when the wall angle is small. However, the $\langle U \rangle$ profile (figure 2*a*) differs significantly from the corresponding SWRG asymptotic field. This may be due to defects in the assumed forms for the $\bar{X}$-dependence of the variables.

Let us now consider the choice of $\bar{Y}_u$ and c_1. As mentioned above, the derivatives of the dependent variables are discontinuous at $\bar{Y} = \bar{Y}_u$, causing stress discontinuities at $\bar{Y} = \bar{Y}_u$. For a specified value of the discharge rate c_1, the value of $\bar{Y}_u$ is chosen so as to minimize the mean stress jump

$$\Delta \equiv (\Delta_{xx} + \Delta_{yy} + \Delta_{xy})/3, \tag{75}$$

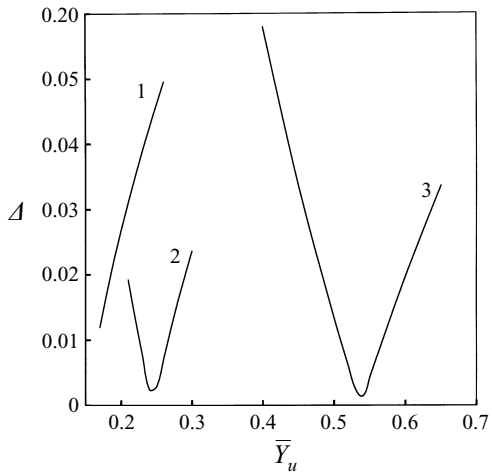

FIGURE 3. Variation of the dimensionless stress jump (defined by equation (75)) with the location of the upstream boundary of the lower frictional–kinetic region: $c_1 = -2.76$ (curve 1), -2.77 (curve 2), -2.80 (curve 3). Parameter values: $\epsilon = 0.024$, $e_p = 0.8$, $k' = 10$, $\bar{Y}_l = -0.3$, the rest as in figure 2.

where

$$\Delta_{xx} = |(\sigma_{xx}(\bar{Y}_u^+) - \sigma_{xx}(\bar{Y}_u^-))/\sigma_{xx}(\bar{Y}_u^+)| \tag{76}$$

is the jump in σ_{xx} at $\bar{Y}_u$, relative to its upstream value. Figure 3 shows that $\bar{Y}_u \simeq 0.24$ for $c_1 = -2.77$ and $\bar{Y}_u \simeq 0.54$ for $c_1 = -2.80$. For $c_1 = -2.76$, reliable results cannot be obtained for $\bar{Y}_u < 0.17$, as the stress singularity is approached. The above procedure generates a suitable value of $\overline{Y}_u$ for each value of the dimensionless mass flow rate c_1. Some procedures for the determination of c_1 are discussed below.

In the frictional models of Davidson & Nedderman (1973), Brennen & Pearce (1978), and Kaza & Jackson (1982*b*), c_1 is fixed by requiring the mean frictional stress σ' to vanish along a traction-free surface spanning the exit slot. Subsequently, Kaza & Jackson (1984) showed that this would result in an unrealistic compaction below the traction-free surface. An alternative approach is to use a free-fall surface (Kaza & Jackson 1982*a*), across which the field variables change discontinuously to attain a state of vertical free fall on the downstream side. This causes a density jump near the exit slot ($\overline{Y} = 0$) (the lower curve in figure 9), in contrast with the smooth variation of the measured density profile (the circles in figure 9). Thus it appears that a satisfactory procedure for the determination of c_1 is not yet available. The procedure used in the present work is indicated below.

The normal stress on the free surface of the particle jet vanishes. Hence one possibility is to require that $\sigma_{n0} = 0$. Here σ_{n0} is the normal stress on the hopper wall, evaluated at the edge of the exit slot ($\overline{X} = 1, \overline{Y} = 0^+$). In the context of a viscous fluid jet issuing from from a circular tube, Tanner, Lam & Bush (1985) used a similar condition to locate the point at which the jet separates from the end of the tube.

In the present case, σ_{n0} decreases from 0.56 to 0.44 as $-c_1$ increases from 2.76 to 2.80. Solutions can be constructed for larger values of $-c_1$, but the following difficulty arises in the lower region $\bar{Y}_u > \bar{Y} \geqslant \bar{Y}_l$ (figure 1). Since (14) is linearized about the upstream solids fraction $\nu = \nu(\bar{Y}_u)$, the mean frictional stress at a critical state (σ_c') becomes negative when ν decreases below a certain value. This happens near the lower boundary $\bar{Y} = \bar{Y}_l$ (figure 4), and larger negative stresses occur as $-c_1$

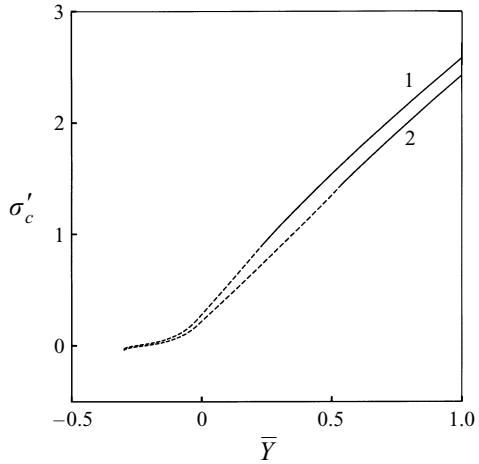

FIGURE 4. Profile of the frictional mean stress at a critical state: —, frictional solution; - -, frictional–kinetic solution, $c_1 = -2.77$, $\overline{Y}_u = 0.24$ (curve 1), $c_2 = -2.80$, $\overline{Y}_u = 0.54$ (curve 2). Parameter values as in figures 2 and 3.

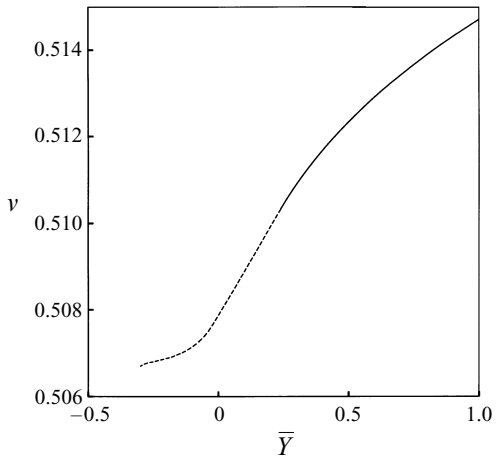

FIGURE 5. Profile of the solids fraction: —, frictional solution; - -, frictional-kinetic solution. Parameter values: $\bar{Y}_u = 0.24$, the rest as in figures 2 and 3.

increases. Since negative values of σ_c' are unacceptable for cohesionless materials, it is not possible within the present framework to examine whether a larger value of $-c_1$ will cause σ_{n0} to vanish.

Here we choose $c_1 = -2.77$ and $\bar{Y}_u = 0.24$, so that the mean stress jump Δ at $\bar{Y} = \bar{Y}_u$ is small ($\simeq 0.2\%$), and σ_c' is positive over most of the domain (figure 4). Results will now be presented for these values of c_1 and $\bar{Y}_u$, and with $\bar{Y}_l = -0.3$. As indicated above, larger values of $|\bar{Y}_l|$ cannot be used due to the occurrence of negative frictional normal stresses.

The value used for c_1 is -2.77, which is close to the incompressible SWRG (smooth wall, radial gravity) estimate for a deep hopper ($= -2.82$). As noted by one of the referees, an alternative estimate of c_1 may be obtained by using a modification (Rose & Tanaka 1959; Nedderman 1992, p. 296) of the correlation due to Beverloo, Liniger & Van de Velde (1961). For $\theta_w = 5^\circ$, this gives $c_1 = -1.71$, which is significantly

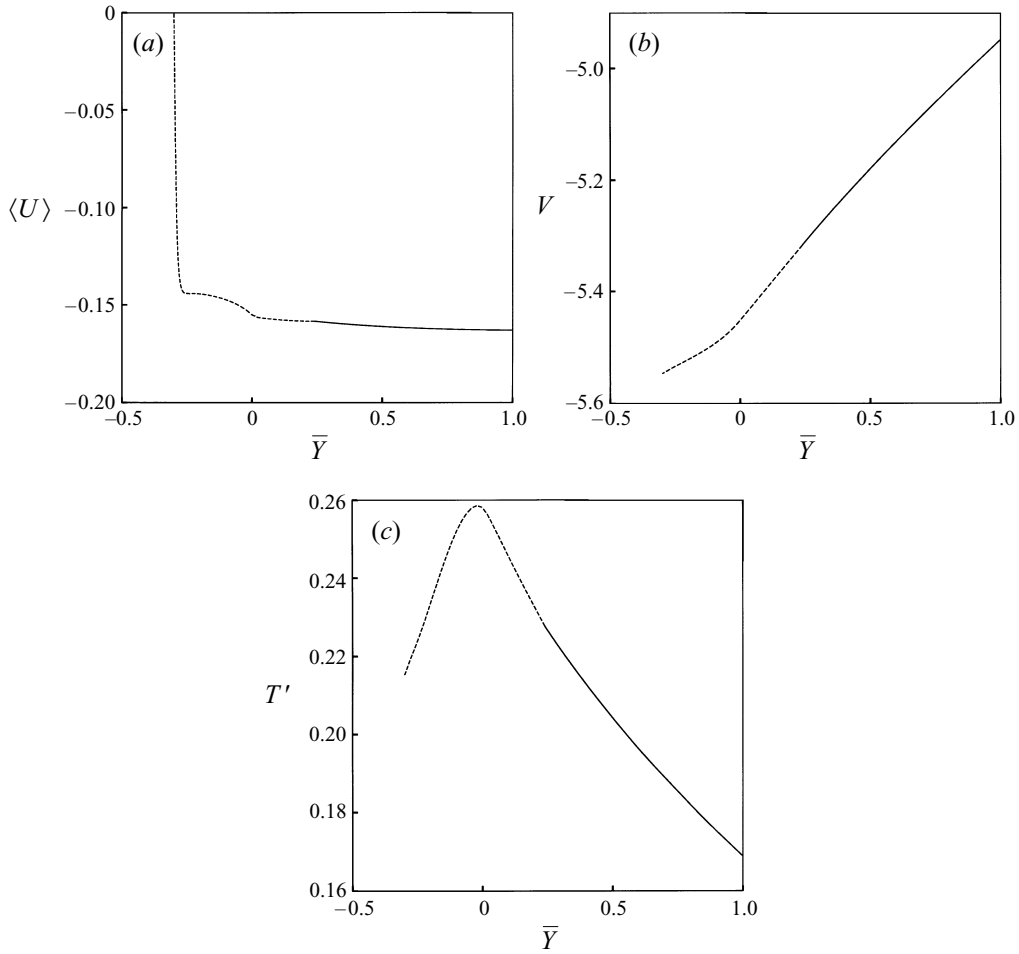

FIGURE 6. Profile of (*a*) the average horizontal velocity, (*b*) the vertical velocity and (*c*) the temperature: —, frictional solution; - -, frictional–kinetic solution. Parameter values: $\bar{Y}_u = 0.24$, the rest as in figures 2 and 3.

smaller in magnitude than the value used in the present work. The discrepancy may be due to the effect of wall roughness. The present results are valid for a hopper with perfectly smooth walls, whereas the correlation of Beverloo *et al.* (1961) has been developed using data for bins. It should be noted that the exit region of a bin behaves effectively like a hopper with rough walls.

The solids fraction decreases as the material flows down the hopper (figure 5), in qualitative agreement with the measurements of Fickie *et al.* (1989) (the circles in figure 9).

Near the hopper exit, the average horizontal velocity $\langle U \rangle$ increases as $\bar{Y}$ decreases (figure 6*a*), in keeping with the tendency of the solution to attain vertical free-fall. This is in contrast with the behaviour in the upper part of the hopper (figure 2*a*). The sharp increase near the lower boundary $\bar{Y} = \bar{Y}_l$ is due to the downstream boundary condition (57). This behaviour could possibly be avoided by applying the downstream conditions at a larger value of $|\bar{Y}_l|$. Since the frictional normal stresses

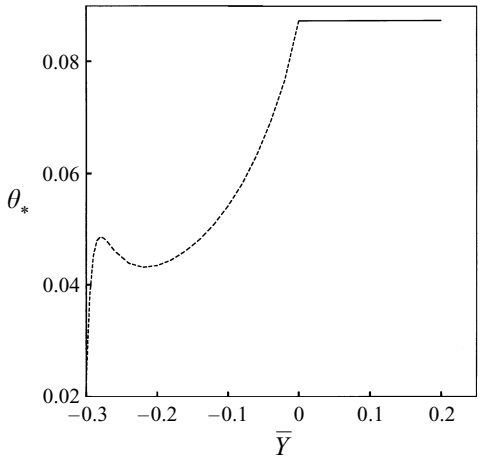

FIGURE 7. Inclination of the free surface of the jet to the vertical (in radians). The horizontal line represents the hopper wall. Parameter values: $\bar{Y}_u = 0.24$, the rest as in figures 2 and 3.

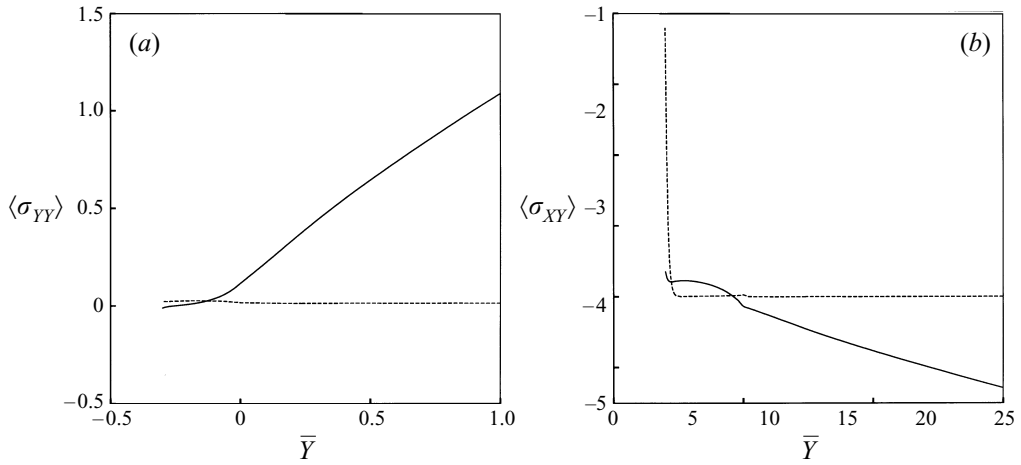

FIGURE 8. Frictional (—) and kinetic (- -) contributions to (*a*) the average normal stress $\langle\sigma_{YY}\rangle$ and (*b*) the average shear stress $\langle\sigma_{XY}\rangle$. Parameter values: $\bar{Y}_u = 0.24$, the rest as in figures 2 and 3.

become negative even for $\bar{Y}_l = -0.3$, larger values of $|\bar{Y}_l|$ cannot be used within the framework of the linearized problem.

The vertical velocity V increases in magnitude as $\bar{Y}$ decreases (figure 6*b*), due to the action of the stress gradients and gravity.

The maximum in the temperature profile (figure 6*c*) is in keeping with our expectation that kinetic effects are important in the exit region. It arises due to a competition between production of pseudo-thermal energy by the working of the viscous stresses, and dissipation of energy due to inelastic collisions and the pressure work associated with dilation.

Figure 7 shows that $\mathrm{d}\theta_*/\mathrm{d}\overline{Y}$, and hence $\mathrm{d}U_*/\mathrm{d}\overline{Y}$, are discontinuous at the hopper exit $\bar{Y} = 0$. The latter discontinuity arises because the variation of the normal stress on the hopper wall does not in general match the *ad hoc* exponential variation prescribed along the 'free surface' of the jet. Hence $\mathrm{d}U_*/\mathrm{d}\overline{Y}\,(0^-)$, obtained by differentiating (65), differs from the upstream value of $\mathrm{d}U_*/\mathrm{d}\overline{Y}(0^+) = \theta_w \mathrm{d}V/\mathrm{d}\overline{Y}\,(0^+)$. At the lower

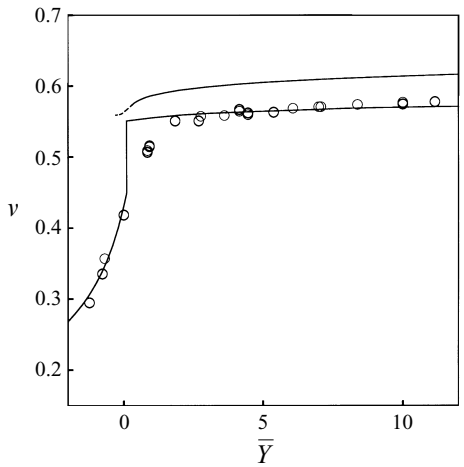

FIGURE 9. Profile of the solids fraction for glass beads: upper curve – present work (—, frictional solution, - -, frictional-kinetic solution), lower curve – results of Prakash & Rao (1991). The circles represent the data of Fickie *et al.* (1989), measured along the centreline of a hopper with $\theta_w = 23^0$. Parameter values: present work – $\theta_w = 5°$, $\rho_p = 2900\,\mathrm{kg\,m^{-3}}$, $\beta = 548$, $\phi = 32.4°$, $\Gamma_1 = 1.47$, $\lambda_1 = 0.049$, $n = 1.03$, $v_1 = 0.52$, $v_{min} = 0.5$, $c_1 = -3.27$, $\epsilon = 0.024$, $e_p = 0.8$, $k' = 10$, $\overline{Y}_u = 0.36$, $\bar{Y}_l = -0.3$, angle of wall friction (ϕ_w) = 0° (smooth walls); Prakash & Rao (1991) – $\theta_w = 23°$, $\rho_p = 2900\,\mathrm{kg\,m^{-3}}$, $\beta = 548$, $\phi = 32.4^0$, $\Gamma_1 = 1.62$, $\lambda_1 = 0.027$, $n = 1.05$, $v_1 = 0$, $\phi_w = 15.1°$.

boundary $\overline{Y} = \overline{Y}_l$, $\theta_* \simeq 0.02$. Therefore, $U_*(\overline{Y}_l) \neq 0$ and the downstream conditions do not strictly correspond to vertical free-fall.

The kinetic stresses are dominated by the frictional stresses, except near the downstream boundary $\bar{Y} = \bar{Y}_l$ (figure 8*a* and 8*b*). The major role of the former is to ensure that the downstream conditions are satisfied, thus ensuring a smooth transition from approximately radial flow in the hopper to vertical free-fall in the jet.

6.2. *Results for glass beads*

Fickie *et al.* (1989) have measured the density profiles for glass beads flowing through a hopper with $\theta_w = 23°$. The experimental value of $\theta_w = 23°$ could not be used directly here, as the iterations associated with the frictional initial value problem did not converge. For $\theta_w = 10°$, a solution can be constructed, but the mean frictional stress σ'_c is negative over a large part of the domain. So results will be presented for $\theta_w = 5°$.

Figure 9 compares the predictions of the present frictional–kinetic model (the upper curve) and the frictional model of Prakash & Rao (1991) (the lower curve) with the data of Fickie *et al.* (1989) (the circles). Let us first consider the present model. The solids fraction profile is qualitatively similar to the data of Fickie *et al.* (1989), but the range of variation is much less than that observed. It remains to be seen whether the model results for $\theta_w = 23°$ and rough walls agree well with the data. Though the model of Prakash & Rao (1991) performs much better than the present model, it has the following defect. It predicts a large density jump near the exit slot ($\overline{Y} = 0$), whereas the data show a smooth variation. On the other hand, the present model predicts a smooth profile, but quantitative agreement is poor.

The data of Fickie *et al.* (1989) (figure 9) raise an intriguing point. Since $v < 0.5$ for $\bar{Y} < 0.8$, the frictional stresses vanish for $\bar{Y} < 0.8$ if the parameter v_{min} in (14)

is chosen as 0.5. Therefore, in the absence of any other stress gradients, free-fall must occur below $\bar{Y} = 0.8$. However, the resulting free-fall trajectories would be incompatible with the geometry of the hopper wall. Thus in the region $0 < \bar{Y} < 0.8$, either the kinetic stresses or forces of some other origin must contribute significantly to the momentum balances, at least near the walls. With the present form of the kinetic equations, this appears possible only if the velocity gradients are of $O(1/\epsilon)$, where ϵ is $\ll 1$. The simple forms (46) assumed for the profiles preclude the occurrence of large gradients in the $\bar{X}$-direction. The two-dimensional model will have to be solved to properly assess the role of the kinetic stresses. Since the kinetic constitutive equations of Lun *et al.* (1984) were developed for small mean field gradients, they may have to be modified along with the flow model, if the observed dilation is to be predicted.

As stated by one of the referees, it is possible that ν_{min}, the value of ν below which frictional effects vanish, is < 0.5. At present, however, the data available from experiments (Richardson 1971, pp. 51–52; Onoda & Liniger 1990) and simulations (Nolan & Kavanagh 1992) suggest that $\nu_{min} \geqslant 0.5$.

7. Discussion

Hybrid frictional–kinetic constitutive equations have been used to develop a model for hopper flow. The resulting equations contain many sources of difficulty, such as a small parameter multiplying the highest derivative, a stress singularity, abrupt change of boundary conditions at the hopper exit, and a free surface which must be determined as a part of the solution. In order to gain some insight, the above equations have been simplified to obtain a quasi-one-dimensional model. The latter shows that it is possible to construct solutions which tend smoothly (barring minor stress jumps at $\bar{Y} = \bar{Y}_u$) from the frictional solution in the hopper to free-fall in the jet. This represents an advance over existing frictional models, which could never be solved satisfactorily in the exit region due to the occurrence of a stress singularity. Within the hopper, the density profile is qualitatively similar to the data of Fickie *et al.* (1989). Near the downstream boundary, the profile is much flatter than that observed. The range of density variation is also underestimated. These defects may be due to the forms of the constitutive equations, and the simplifying assumptions used in model formulation.

Overall, the use of a hybrid frictional–kinetic model appears to be promising. However, there is considerable scope for refinement, both with regard to the model proposed and the constitutive equations used. In this context, the present work may be regarded as a small step towards the solution of an outstanding problem in granular flow.

We are grateful to the referees for many constructive comments, to Professor R. Jackson for sending us the raw density data of Fickie *et al.* (1989), and to Dr Prabhu Nott for helpful discussions.

Appendix A. Asymptotic fields for compressible flow through a smooth-walled hopper with radial gravity

An interesting and useful feature of the frictional equations for hopper flow is the existence of asymptotic density, velocity, and stress fields. These fields are independent of the boundary conditions specified far upstream. They are likely to be applicable even in the frictional–kinetic case, since far above the exit the kinetic

stresses are expected to be very small. Further, asymptotic temperature fields have been constructed for the incompressible frictional–kinetic SWRG problem (Jyotsna & Rao 1991), and are expected in the compressible case too. This is indeed true as will be seen shortly.

The asymptotic fields are of interest, since they can be used to generate upstream conditions for the solution of the frictional–kinetic equations in the exit region of the hopper. In particular, the fields for the SWRG problem are useful for the problem of flow through a smooth-walled hopper with steep walls. This is because the fields for the former are easy to determine, and are also expected to be a fairly good approximation to the asymptotic solution for the latter.

Far above the hopper exit, it is reasonable to assume that both inertial and kinetic terms are negligible in the momentum balances. Further, from the results of Jyotsna & Rao (1991), conduction may be neglected in the energy balance. Thus, the asymptotic fields are determined from the mass balance, momentum balances with inertial and kinetic terms omitted, and the conduction-free energy balance.

Using polar coordinates with origin located at the apparent vertex of the hopper, the relevant frictional equations admit a solution wherein all the dependent variables are functions of the dimensionless radial coordinate $\xi' = r/w$.

The asymptotic solids fraction and velocity fields are constructed using a perturbation method due to Prakash & Rao (1991). This generates a series solution in powers of λ_1, where λ_1 is a parameter occurring in (12). The two-term solution is given by

$$v' = \frac{-c_1}{\xi' \theta_w} \left[-\Gamma_1 + \lambda_1 \ln\left(\frac{s_1 \xi'}{\beta}\right)\right], \tag{A 1}$$

$$v = \frac{1}{\Gamma_1} + \left(\frac{\lambda_1}{{\Gamma_1}^2}\right) \ln\left(\frac{s_1 \xi'}{\beta}\right), \tag{A 2}$$

where $v' = v_r/(gw)^{1/2}$ is the dimensionless radial velocity, and $s_1 = 1/(\Gamma_1(3\sin\phi - 1))$.

We now determine the asymptotic temperature field, if any, for the compressible frictional–kinetic problem. In polar coordinates, the conduction-free energy balance is given by

$$\tfrac{3}{2} v v' \frac{\mathrm{d}T'}{\mathrm{d}\xi'} + \left[h_1 T' - h_2 T'^{1/2}\left(\frac{\mathrm{d}v'}{\mathrm{d}\xi'} + \frac{v'}{\xi'}\right)\right]\left[\frac{\mathrm{d}v'}{\mathrm{d}\xi'} + \frac{v'}{\xi'}\right] - \tfrac{4}{3} h_3 T'^{1/2}\left[\left(\frac{\mathrm{d}v'}{\mathrm{d}\xi'}\right)^2 + \left(\frac{v'}{\xi'}\right)^2 - \frac{\mathrm{d}v'}{\mathrm{d}\xi'}\frac{v'}{\xi'}\right] + h_6 T'^{3/2} = 0, \tag{A 3}$$

where the functions h_i are defined in table 1. Since the h_i are sensitive functions of v, we use a three-term solution to the solids fraction field instead of (A 2). Thus

$$v = \frac{1}{\Gamma_1} + \left(\frac{\lambda_1}{{\Gamma_1}^2}\right)\ln\left(\frac{s_1 \xi'}{\beta}\right) + \frac{{\lambda_1}^2}{{\Gamma_1}^3}\left[\ln\left(\frac{s_1\xi'}{\beta}\right)\left(1 + \ln\left(\frac{s_1\xi'}{\beta}\right)\right) + s_2 - \frac{s_1\Gamma_1(n-1)}{2n\sin\phi}\right], \tag{A 4}$$

where $s_2 = (1 - \sin\phi)/(3\sin\phi - 1)$ and n is a parameter occurring in (13).

Equations (A 1) and (A 4) are used to solve the energy balance (A 3). Unlike the solutions for v and v', a perturbation method cannot be used for the temperature field, owing to the following difficulty. As part of the perturbation scheme, the functions $h_i(v)$ are linearized about the zero-order solution for v, i.e. about $v = 1/\Gamma_1$. For the

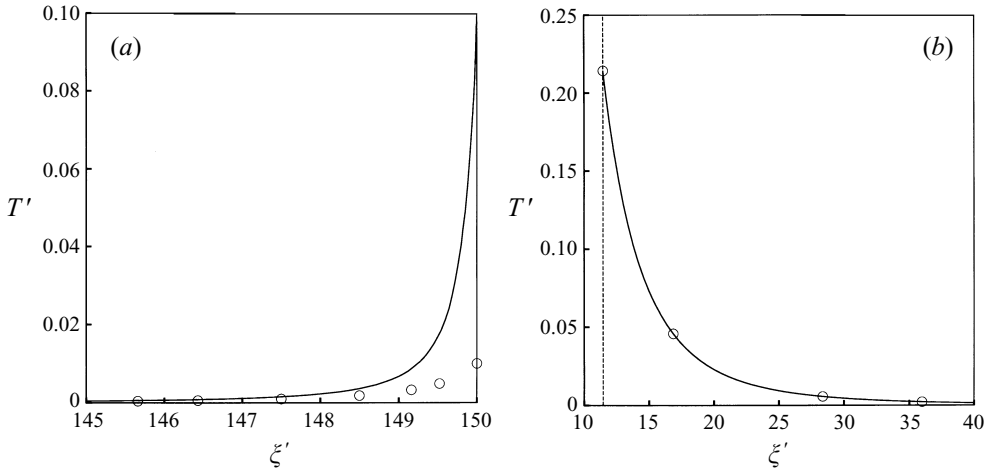

FIGURE 10. Profile of the temperature for the SWRG problem (*a*) near $\xi' = r/w = 150$, and (*b*) near the hopper exit: —, $T_i \equiv T'(\xi' = 150) = 0.1$; ○, $T_i = 0.01$. Here $\xi' = (Y + \cot\theta_w)/\cos\theta \simeq Y + (1/\theta_w)$ in view of the small angle approximation (§ 3.1), and θ is the angle measured from the vertical to any radial line drawn from the apparent vertex of the hopper. The broken vertical line represents the exit slot. Parameter values as in figures 2 and 3.

value of $\Gamma_1 = 1.47$ estimated from the data of Fickie *et al.* (1989) (see § A 1), $1/\Gamma_1$ exceeds ν_0, the volume fraction of solids for a random close packing. For $\nu > \nu_0$, the functions h_i cannot be evaluated, since the radial distribution function g_0 is not defined in this range. Therefore, instead of using a perturbation method, the energy balance is solved numerically using a semi-implicit Runge–Kutta method (Villadsen & Michelsen 1978, pp. 319–323).

For Leighton Buzzard sand, the temperature profiles obtained for different 'initial' values of T' (specified at $\xi' = 150$) asymptote to a common one nearly immediately below the upstream boundary (figure 10). Here the initial value of ξ' is chosen as 150 to ensure that the integration is started sufficiently far above the hopper exit for the asymptotic solution to be reached. For glass beads, a similar asymptotic behaviour is observed when the initial values are specified at $\xi' = 50$.

Thus the asymptotic fields for the compressible frictional–kinetic SWRG problem are given by (A 1), (A 4), and the numerical solution of the conduction-free energy balance.

A.1. *Estimation of the parameters Γ_1 and λ_1 for glass beads*

The values of Γ_1 and λ_1 are estimated by fitting the asymptotic solids fraction field to the data of Fickie *et al.* (1989). The experiments were conducted in a hopper with aluminium walls. Since (A 2) has been derived for the case of smooth walls, it cannot be directly used with the data. When the assumptions of smooth walls and radial gravity are relaxed, (A 2) may be replaced by (Prakash & Rao, 1991)

$$\nu = \frac{1}{\Gamma_1} + \left(\frac{\lambda_1}{{\Gamma_1}^2}\right) \ln\left(\frac{s_3(\theta)\ \xi'}{\beta}\right), \tag{A 5}$$

where the function $s_3(\theta)$ is obtained by numerical integration of ordinary differential equations corresponding to the incompressible radial stress field (Jenike 1961, 1964), and θ is the angle measured from the vertical (as in figure 1). Since the density measured along the centreline is used for parameter estimation, we set $\theta = 0$ in (A 5).

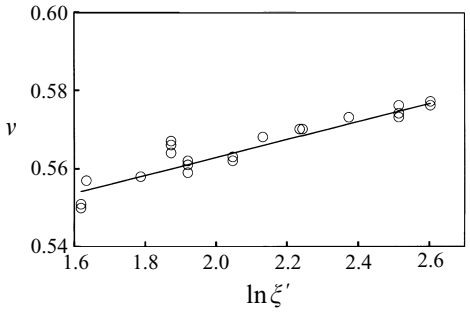

FIGURE 11. Fit of SWRG asymptotic solids fraction profile (A 7) (—) to the data (○) of Fickie *et al.* (1989). Parameter values: $\theta_w = 23°$, $\beta = 548$, $\phi = 32.4°$, $\phi_w = 15°$ ($\gamma_w = 23.1°$), $\Gamma_1 = 1.47$, $\lambda_1 = 0.049$.

Further, $s_3(0)$ is approximated by the solution due to Brennen & Pearce (1978) to get

$$s_3(0) = \frac{1}{\Gamma_1(3\sin\phi - 1 + 2(\gamma_w/\theta_w)\sin\phi)}. \tag{A 6}$$

Here $\gamma_w = \gamma(\theta = \theta_w)$ can be calculated once the values of the angle of internal friction ϕ and the angle of wall friction ϕ_w are specified (Brennen & Pearce 1978). In the limit of smooth walls ($\gamma_w = 0$), (A 5) reduces to (A 2).

To estimate the values of Γ_1 and λ_1, (A 5) is rewritten as

$$v = a + b\ (\ln \xi'), \tag{A 7}$$

where

$$a = \frac{1}{\Gamma_1} + \frac{\lambda_1}{\Gamma_1^2} \ln\left(\frac{s_3(0)}{\Gamma_1 \beta}\right);\ b = \frac{\lambda_1}{\Gamma_1^2}.$$

The constants a and b are estimated using the method of least squares, and the above equations are then solved iteratively to obtain the values of Γ_1 and λ_1.

The angle of wall friction ϕ_w for glass beads flowing past an aluminium wall is taken as 15° (R. Jackson 1989, private communicaton). Using the density data in the range $1.6 < \ln \xi' < 2.6$, and setting $\phi = 32.4°$ (see § 5), we get $\Gamma_1 = 1.47$ and $\lambda_1 = 0.049$. The fit to the data is shown in figure 11. It is interesting to note that the values of Γ_1 and λ_1 are of the same order as those used by Thorpe (1992), namely $\Gamma_1 = 1.38$ and $\lambda_1 = 0.064$. The latter differ from the present values because they were estimated using a slightly different approach.

REFERENCES

ACKERMANN, N. L. & SHEN, H. 1982 Stresses in rapidly sheared fluid-solid mixtures. *J. Engng Mech., Proc. ASCE* **108**, 95–113.

AHMADI, G. & SHAHINPOOR, M. 1984 A kinetic model for rapid flows of granular materials. *Intl J. Non-linear Mech.* **19**, 177–186.

AIREY, D. W., BUDHU, M. & WOOD, D. M. 1985 Some aspects of the behaviour of soils in simple shear. In *Developments in Soil Mechanics and Foundation Engineering-2* (ed. P. K. Banerjee & R. Butterfield), pp. 185–213. Elsevier.

ALDER, B. J. & WAINWRIGHT, T. E. 1960 Studies in molecular dynamics. II. Behaviour of a small number of elastic spheres. *J. Chem. Phys.* **33**, 1439–1451.

ANDERSON, K. G. & JACKSON, R. 1992 A comparison of the solution of some proposed equations of motion of granular materials for fully developed flow down inclined planes. *J. Fluid Mech.* **241**, 145–168.

ATKINSON, J. H. & BRANSBY, P. L. 1978 *The Mechanics of Soils.* McGraw-Hill.

Beverloo, W. A., Liniger, H. A. & Van de Velde, J. 1961 The flow of granular solids through orifices. *Chem. Engng Sci.* **15**, 260–269.

Blair-Fish, P. M. & Bransby, P. L. 1973 Flow patterns and wall stresses in a mass flow bunker. *Trans. ASME* B: *J. Engng Ind.* **95**, 17–26.

Bosley, J., Schofield, C. & Shook, C. A. 1969 An experimental study of granule discharge from model hoppers. *Trans. Inst. Chem. Engrs* **47**, T147–T153.

Boyle, E. J. & Massoudi, M. 1990 A theory for granular materials exhibiting normal stress effects based on Enskog's dense gas theory. *Intl J. Engng Sci.* **28**, 1261–1275.

Brennen, C. & Pearce, J. C. 1978 Granular material flow in two-dimensional hoppers. *Trans. ASME* E: *J. Appl. Mech.* **45**, 43–50.

Brown, R. L. & Richards, J. C. 1970 *Principles of Powder Mechanics.* Pergamon.

Cao, J., Ahmadi, G. & Massoudi, M. 1996 Gravity flows of slightly frictional particles down an inclined bumpy chute. *J. Fluid Mech.* **316**, 197–222.

Darton, R. C. 1976 The structure and dispersion of jets of solid particles falling from a hopper. *Powder Technol.* **13**, 241–250.

Davidson, J. F. & Nedderman, R. M. 1973 The hour glass theory of hopper flow. *Trans. Instn Chem. Engrs* **51**, 29–35.

Ding, J. & Gidaspow, D. 1990 A bubbling fluidization model using kinetic theory of granular flow. *AIChE J.* **36**, 523–538.

Fickie, K. E., Mehrabi, R. & Jackson, R. 1989 Density variations in a granular material flowing from a wedge-shaped hopper. *AIChE J.* **35**, 853–855.

Goldshtein, A. & Shapiro, M. 1995 Mechanics of collisional motion of granular materials. Part 1. General hydrodynamic equations. *J. Fluid Mech.* **282**, 75–114.

Goldshtein, A., Shapiro, M., Moldavsky, L. & Fichman, M. 1995 Mechanics of collisional motion of granular materials. Part 2. Wave propagation through a granular layer. *J. Fluid Mech.* **287**, 349–382.

Goodman, M. A. & Cowin, S. C. 1971 Two problems in the gravity flow of granular materials. *J. Fluid Mech.* **45**, 321–339.

Haff, P. K. 1983 Grain flow as a fluid mechanical phenomenon. *J. Fluid Mech.* **134**, 401–430.

Hankey, W. L. & Thomas, S. K. 1991 The flow of granular material. *Computers and Fluids* **20**, 333-342.

Jackson, R. 1983 Some mathematical and physical aspects of continuum models for the motion of granular materials. In *Theory of Dispersed Multiphase Flow* (ed. R. E. Meyer), pp. 291–337. Academic.

Jenike A. W. 1961 Gravity flow of bulk solids. *Bulletin* 108. Univ. Utah Engng Expt. Station.

Jenike A. W. 1964 Steady gravity flow of frictional cohesive solids in converging channels. *Trans. ASME* E: *J. Appl. Mech.* **31**, 5–11.

Jenkins, J. T. & Richman, M. W. 1985 Grad's 13-moment system for a dense gas of inelastic spheres. *Arch. Rat. Mech. Anal.* **87**, 355–377.

Jenkins, J. T. & Savage, S. B. 1983 A theory for the rapid flow of identical, smooth, nearly elastic, spherical particles. *J. Fluid Mech.* **130**, 187–202.

Johnson, P. C. & Jackson, R. 1987 Frictional-collisional constitutive relations for granular materials, with application to plane shearing. *J. Fluid Mech.* **176**, 67–93.

Johnson, P. C., Nott, P. & Jackson, R. 1990 Frictional-collisional equations of motion for particulate flows and their application to chutes. *J. Fluid Mech.* **210**, 501–535.

Jyotsna, R. & Rao, K. K. 1991 Steady incompressible flow of cohesionless granular materials through a wedge-shaped hopper: frictional-kinetic solution to the smooth wall, radial gravity problem. *Chem. Engng Sci.* **46**, 1951–1967.

Kaza, K. R. 1982 The mechanics of flowing granular materials. PhD thesis, University of Houston.

Kaza, K. R. & Jackson, R. 1982*a* A problem in the flow of granular materials. *Proc. 9th US Natl Congress on Applied Mechanics.*

Kaza, K. R. & Jackson, R. 1982*b* The rate of discharge of coarse granular material from a wedge-shaped mass flow hopper. *Powder Technol.* **33**, 223–237.

Kaza, K. R. & Jackson, R. 1984 Boundary conditions for a granular material flowing out of a hopper or bin. *Chem. Engng Sci.* **39**, 915–916.

Lun, C. K. K. 1991 Kinetic theory for granular flow of dense, slightly inelastic, slightly rough spheres. *J. Fluid Mech.* **233**, 539–559.

Lun, C. K. K. & Savage, S. B. 1987 A simple kinetic theory for granular flow of rough, inelastic, spherical particles. *Trans. ASME* E: *J. Appl. Mech.* **54**, 47–53.

Lun, C. K. K., Savage, S. B., Jeffrey, D. J. & Chepurniy, N. 1984 Kinetic theories for granular flow: inelastic particles in Couette flow and slightly inelastic particles in a general flowfield. *J. Fluid Mech.* **140**, 223–256.

Ma, D. & Ahmadi, G. 1986 An equation of state for dense rigid sphere gases. *J. Chem. Phys.* **84**, 3449–3450.

Ma, D. & Ahmadi, G. 1988 A kinetic model for rapid granular flows of nearly elastic particles including interstitial fluid effects. *Powder Technol.* **56**, 191–207.

Mctigue, D. F. 1978 A model for stresses in shear flow of granular materials. In *Proc. US-Japan Seminar on Continuum-Mechanical and Statistical Approaches in the Mechanics of Granular Materials* (ed. S. C. Cowin & M. Satake), pp. 266–271. Gakujutsu Bunken Fukyukai.

Meric, R. A. & Tabarrok, B. 1982 On the gravity flow of granular materials. *Intl J. Mech. Sci.* **24**, 469–478.

Nedderman, R. M. 1992 *Statics and Kinematics of Granular Materials*. Cambridge University Press.

Nedderman, R. M., Tüzün, U., Savage, S. B. & Houlsby, G. T. 1982 The flow of granular materials-I. *Chem. Engng Sci.* **37**, 1597–1609.

Nolan, G. T. & Kavanagh, P. E. 1992 Computer simulation of random packing of hard spheres. *Powder Technol.* **72**, 149–155.

Onoda, G. Y. & Liniger, E. G. 1990 Random loose packings of uniform spheres and the dilatancy onset. *Phys. Rev. Lett.* **64**, 2727–2730.

Passman, S. L., Jenkins, J. T. & Thomas, J. P. 1978 Flow of granular material in a vertical channel. In *Proc. US-Japan Seminar on Continuum-Mechanical and Statistical Approaches in the Mechanics of Granular Materials* (ed. S. C. Cowin & M. Satake), pp. 171–180. Gakujutsu Bunken Fukyukai.

Pitman, E. B. & Schaeffer, D. G. 1987 Stability of time dependent compressible granular flow in two dimensions. *Commun. Pure Appl. Maths* **40**, 421–447.

Potanin, A. A. 1992 On models of granular material flow under dynamic conditions. *Powder Technol.* **69**, 107–117.

Prakash, J. R. & Rao, K. K. 1988 Steady compressible flow of granular materials through a wedge-shaped hopper: the smooth wall, radial gravity problem. *Chem. Engng Sci.* **43**, 479–494.

Prakash, J. R. & Rao, K. K. 1991 Steady compressible flow of cohesionless granular materials through a wedge-shaped hopper. *J. Fluid Mech.* **225**, 21–80.

Rathbone, T., Nedderman, R. M. & Davidson, J. F. 1987 Aeration, deaeration, and flooding of fine particles. *Chem. Engng Sci.* **42**, 725–736.

Richardson, J. F. 1971 Incipient fluidisation and particulate systems. In *Fluidization* (ed. J. F. Davidson & D. Harrison), pp. 25–64. Academic.

Rose, H. E. & Tanaka, T. 1959 Rate of discharge of granular materials from bins and hoppers. *The Engineer* **208**, 465–469.

Savage, S. B. 1965 The mass flow of granular material from coupled velocity-stress fields. *Br. J. Appl. Phys.* **16**, 1885–1888.

Savage, S. B. 1979 Gravity flow of cohesionless granular materials in chutes and channels. *J. Fluid Mech.* **92**, 53–96.

Savage, S. B. 1983 Granular flows down rough inclines - review and extension. In *Mechanics of Granular Materials: New Models and Constitutive Relations* (ed. J. T. Jenkins & M. Satake), pp. 261–282. Elsevier.

Savage, S. B. 1988 Streaming motions in a bed of vibrationally fluidised dry granular material. *J. Fluid Mech.* **194**, 457–478.

Savage, S. B. & Jeffrey, D. J. 1981 The stress tensor in a granular flow at high shear rates. *J. Fluid Mech.* **110**, 255–272.

Sayed, M. & Savage, S. B. 1983 Rapid gravity flow of cohesionless granular materials down inclined chutes. *Z. Angew Math. Phys.* **34**, 84–99.

Schreier, S. 1982 *Compressible Flow*. John Wiley.

Spencer, A. J. M. 1982 Deformation of an ideal granular material. In *Mechanics of Solids* (ed. H. G. Hopkins & M. J. Sewell), pp. 607–652. Pergamon.

Szidarovszky, F., Hutter, K. & Yakowitz, S. 1987 A numerical study of steady plane granular

chute flows using the Jenkins-Savage model and its extension. *Intl J. Num. Meth. Engng* **24**, 1993–2015.

Tanner, R. I., Lam, H. & Bush, M. B. 1985 The separation of viscous jets. *Phys. Fluids* **28**, 23–25.

Thorpe, R. B. 1992 An experimental clue to the importance of dilation in determining the flow rate of a granular material from a hopper or bin. *Chem. Engng Sci.* **47**, 4295–4303.

Van Zuilichem, D. J., Van Egmond, N. D. & De Swart, J. G. 1974 Density behaviour of flowing granular material. *Powder Technol.* **10**, 161–169.

Villadsen, J. & Michelsen, M. L. 1978 *Solution of Differential Equation Models by Polynomial Approximation.* Prentice-Hall.

Yalamanchili, R. C., Gudhe, R. & Rajagopal, K. R. 1994 Flow of granular materials in a vertical channel under the action of gravity. *Powder Technol.* **81**, 65–73.

Zienkiewicz, O. C. 1977 *The Finite Element Method*. McGraw-Hill.